

AD-A065 126

ELECTRONIC VISION CO SAN DIEGO CA
ICCD SENSITIVITY INVESTIGATION.(U)
JUN 78 R O 6INAVEN
SAI-78-730-EVC

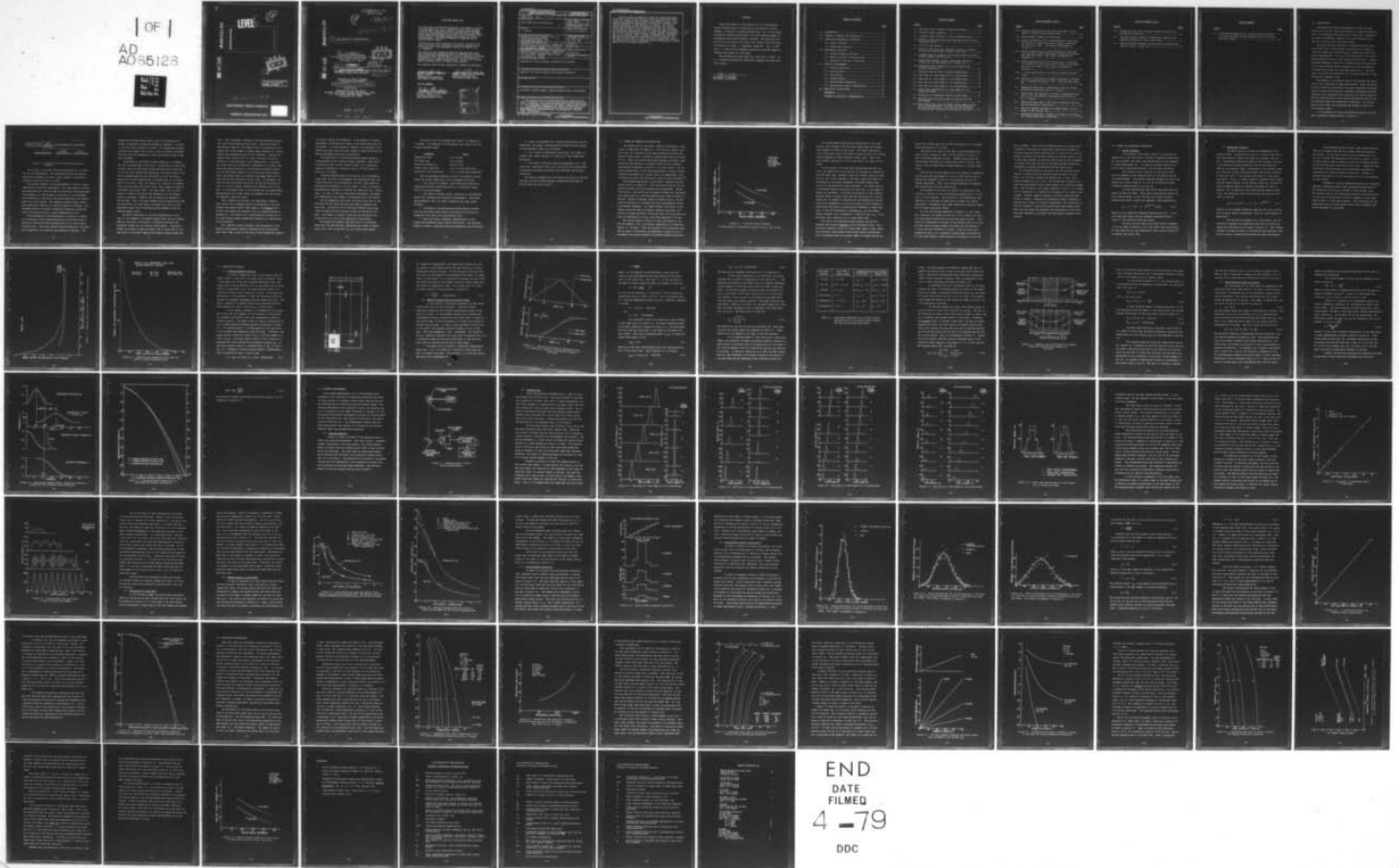
F/G 17/8

UNCLASSIFIED

SAMSO-TR-79-1

F04701-77-C-0058
NL

1 OF 1
AD
AD55123

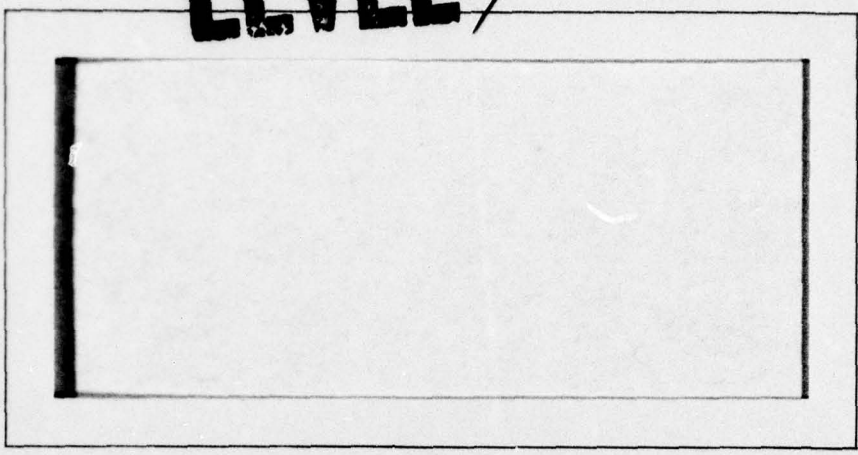


2

12

LEVEL

AD A0 651 26



DDC FILE COPY

DDC
MAR 1 1979
C

This document has been approved for public release and sale; its distribution is unlimited.

79 02 23 022

ELECTRONIC VISION COMPANY

SCIENCE APPLICATIONS, INC.



ADA065126

DDC FILE COPY

18 SAMS0 TR NO. 79-1
SAI-78-730-EVC

12

19 TR-79-11

14 SAI-78-730-EVC

6 ICCD SENSITIVITY INVESTIGATION.

10 R. O. Ginaven
Electronic Vision Company

A Division of Science Applications, Inc
11526 Sorrento Valley Road
San Diego, CA 92121

DDC
RECEIVED
MAR 1 1979

11 22 Jun 1978

12 89p.

9 FINAL TECHNICAL REPORT, Aug 77 - Jun 78,
FOR PERIOD AUGUST 1977-JUNE 1978

16 2132

Approved for Public Release;
Distribution Unlimited

15 F04701-77-C-0058

Prepared For:

Department of the Air Force
Hq Space and Missile Systems Organization (AFSC)
P.O. Box 92960, Worldway Postal Center
Los Angeles, CA 90009

390 074

JOB

79 02 23 022


REVIEW AND APPROVAL PAGE

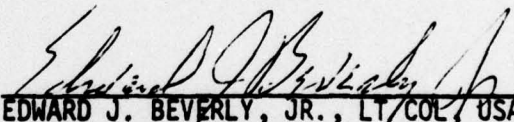
This final report was submitted by Electronic Vision Company, a division of Science Applications, Inc., 11526 Sorrento Valley Road, San Diego, California 92121, under Contract F04701-77-C-0058 with the Department of the Air Force, Hq Space and Missile Systems Organization (Hq SAMSO) (AFSC), Space Defense Systems Program Office (YN), Directorate of Survivability (YNV), P.O. Box 92960, Worldway Postal Center, Los Angeles, California 90009. Capt Joseph E. Hernandez, HQ SAMSO/YNV, was the Project Officer in charge.

The views and conclusions contained in this document are those of the authors and should not be interpreted as necessarily representing the official policies, either expressed or implied, of Hq SAMSO or the U.S. Government.


This report has been reviewed and cleared for open publication and/or public release by the appropriate Office of Information (OI) in accordance with AFR 190-17 and DODD 5230.9. There is no objection to unlimited distribution of this report to the public at large, or by DDC to the National Technical Information Service (NTIS). At NTIS it will be available to the general public, including foreign nationals.

This technical report has been reviewed and is approved for publication.


JOSEPH E. HERNANDEZ, CAPT, USAF
Project Officer
Directorate of Survivability
Space Defense Systems Program


EDWARD J. BEVERLY, JR., LT COL, USAF
Director of Survivability
Space Defense Systems Program

FOR THE COMMANDER


RICHARD G. DINGMAN, Colonel, USAF
Assistant Program Director
Space Defense Systems Program

ACCESSION for	
NTIS	White Section <input checked="" type="checkbox"/>
DDC	Buff Section <input type="checkbox"/>
UNANNOUNCED JUSTIFICATION	<input type="checkbox"/>
BY	
DISTRIBUTION/AVAILABILITY CODES	
Dist.	SPECIAL
A	

Unclassified

SECURITY CLASSIFICATION OF THIS PAGE (When Data Entered)

REPORT DOCUMENTATION PAGE		READ INSTRUCTIONS BEFORE COMPLETING FORM
1. REPORT NUMBER SAMSO TR No. 79-1	2. GOVT ACCESSION NO.	3. RECIPIENT'S CATALOG NUMBER
4. TITLE (and Subtitle) ICCD Sensitivity Investigation	5. TYPE OF REPORT & PERIOD COVERED Final Report August 1977-June 1978	
	6. PERFORMING ORG. REPORT NUMBER SAI-78-730-EVC	
7. AUTHOR(s) R. Ginaven	8. CONTRACT OR GRANT NUMBER(s) F04701-77-C-0058 <i>ml</i>	
9. PERFORMING ORGANIZATION NAME AND ADDRESS Electronic Vision Company, A Div. of Science Applications, Inc. 11526 Sorrento Valley Road San Diego, CA 92121	10. PROGRAM ELEMENT, PROJECT, TASK AREA & WORK UNIT NUMBERS PE 63438F, Proj. 2132 Work Unit #DF	
11. CONTROLLING OFFICE NAME AND ADDRESS Department of the Air Force, Hq Space and Missile Systems Organization (AFSC)/YNV, P.O. Box 92960, Worldway Postal Center Los Angeles, CA 90009	12. REPORT DATE 78 June 22	
	13. NUMBER OF PAGES 78	
14. MONITORING AGENCY NAME & ADDRESS (if different from Controlling Office) Department of the Air Force, Hq Space and Missile Systems Organization (AFSC)/YNV, P.O. Box 92960, Worldway Postal Center Los Angeles, CA 90009	15. SECURITY CLASS. (of this report) Unclassified	
	15a. DECLASSIFICATION/DOWNGRADING SCHEDULE	
16. DISTRIBUTION STATEMENT (of this Report) Approved for Public Release; Distribution Unlimited.		
17. DISTRIBUTION STATEMENT (of the abstract entered in Block 20, if different from Report) Approved for Public Release; Distribution Unlimited.		
18. SUPPLEMENTARY NOTES		
19. KEY WORDS (Continue on reverse side if necessary and identify by block number) Satellite, optical sensor, charge coupled device, and Digicon.		
20. ABSTRACT (Continue on reverse side if necessary and identify by block number) The sensitivity of an Intensified Charge Coupled Device (ICCD) utilizing a CCD to detect photoelectrons has been evaluated for operating conditions anticipated in space applications. Data processing techniques for signal discrimination have been identified and evaluated using simulated star scanning measurements and estimated signal and background (zodiacal light) intensities.		

Unclassified

★ Unclassified

SECURITY CLASSIFICATION OF THIS PAGE(When Data Entered)

Since the ICCD is capable of detecting single photoelectrons with a high signal-to-noise ratio, the practical sensitivity is limited by the intensity of background light. The background produces signals which occasionally exceed the detection threshold in the absence of a target. The rate of these "background events" has been calculated for various conditions and found to be acceptably low even for detection of relatively faint objects (visual magnitude, $m_v = 8$) with a high detection probability (99%) in quite intense backgrounds (up to -1.2 stellar magnitudes per square degree) corresponding to the zodiacal light at about 10 degrees from the sun, provided that scattering and diffraction of sunlight at 10° off axis is less than -1.2 m_v . At larger angles from the sun, the background intensity drops rapidly and considerably fainter objects can be reliably detected.

dec

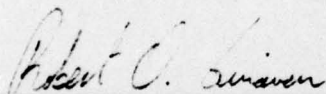
Unclassified

SECURITY CLASSIFICATION OF THIS PAGE(When Data Entered)

FOREWARD

This final report on the sensitivity of an Intensified Charge Coupled Device is submitted by the Electronic Vision Company, a Division of Science Applications, Inc., to the Space and Missile Systems Organization, Air Force Systems Command in accordance with Contract F04701-77-C-0058. The study was conducted over the period from August 1977 through June 1978 under the direction of Capt. J. Hernandez, SAMSO/YNV. Drs. S. Kash and N. C. Chang of the Aerospace Corporation provided technical guidance and support for the study.

The scanning data were taken by G. Hall and L. Acton. Dr. R. O. Ginaven performed the sensitivity analysis and wrote the final report.



Dr. Robert O. Ginaven
Principal Investigator

TABLE OF CONTENTS

	<u>Page</u>
1.0 INTRODUCTION.....	1
2.0 SUMMARY OF RESULTS AND CONCLUSIONS.....	8
3.0 TARGET AND BACKGROUND INTENSITIES.....	13
3.1 Target Intensity.....	13
3.2 Background Intensity.....	14
4.0 SENSITIVITY ANALYSIS.....	18
4.1 Scanning Geometry and Rate.....	18
4.2 Effect of Motion on Target Signal.....	20
4.3 Background Event Rate Calculation.....	28
5.0 SCANNING MEASUREMENTS.....	33
5.1 Scanning Apparatus.....	33
5.2 Scanning Data.....	35
5.3 Peak Signals.....	45
5.4 Average Signals.....	46
5.5 Shift-and-Add Integration.....	49
5.6 Photoelectron Signal Distributions.....	51
6.0 SENSITIVITY CALCULATIONS.....	60
REFERENCES.....	75
GLOSSARY OF NOTATION & ABBREVIATIONS.....	76

LIST OF FIGURES

<u>Figure</u>	<u>Page</u>
1.1 Functional Block Diagram of Detection System.....	2
2.1 Limiting Target Intensity.....	9
3.1 Zodiacal Light Intensity vs Solar Elongation Angle.....	16
3.2 Zodiacal Light Background Count Rate per Pixel vs Solar Elongation Angle.....	17
4.1 ICCD Scanning Geometry.....	19
4.2 Relative Count Rate and Integrated Count as a Function of Time as a Moving Spot Crosses a CCD Pixel.....	21
4.3 Geometry Used to Calculate the Average Signal per Frame as Spot Crosses the CCD Array.....	26
4.4 Relationship Between Signal, Background, Detection Probability and Background Even Probability.....	30
4.5 Background Event Probability vs Q for Normal and Poisson Distribution.....	31
5.1 Apparatus Used to Obtain Scanning Measurements.....	34
5.2 Scan Data at a Scan Speed of 0.15 Pixels/Frame.....	36
5.3 Scan Data at a Scan Speed of 0.54 Pixels/Frame.....	37
5.4 Scan Data at a Scan Speed of 0.9 Pixels/Frame.....	38
5.5 Scan Data at a Scan Speed of 2.44 Pixels/Frame.....	39
5.6 Signal Time Distribution at a Scan Speed of 0.15 Pixels per Frame.....	40
5.7 Reciprocal of Integrated Signals vs Scan Speed.....	43
5.8 Maximum Signal from Each Frame vs Time for Various Scan Speeds.....	44
5.9 Peak Signals per pixel per frame vs Scan Speed for CCD 202 and Contiguous CCD. The data for the contiguous CCD were derived analytically from the CCD 202 data.....	47

LIST OF FIGURES (Cont.)

<u>Figure</u>	<u>Page</u>
5.10 Relative Average Signal per pixel per frame vs Scan Speed for CCD 202 and Contiguous CCD.....	48
5.11 Shift-and-Add Integration Simulation.....	50
5.12 Signal Distribution for 18 keV Electrons in One Pixel of CCD 202 at a Mean Flux Rate of About 4 Electrons per pixel per frame. Zero signal corresponds to channel 33.....	52
5.13 Signal Distribution for 18 keV Electrons in One Pixel of a CCD 202 at a Mean Flux Rate of About 14 Electrons per pixel per frame. Zero signal corresponds to channel 33.....	53
5.14 Signal Distribution for 18 keV Electrons in One Pixel of a CCD 202 at a Mean Flux Rate of About 25 Electrons per pixel per frame. Zero signal corresponds to channel 33.....	54
5.15 σ^2 vs Net Peak Position for Electron Signal Distributions.....	57
5.16 Fraction of Distribution Exceeding Threshold vs Threshold in Standard Deviations (\sqrt{N}) from the Mean Value (N).....	59
6.1 Background Event Rate vs Observation Time for Various Background Intensities and $M_V = 6$ Target.....	62
6.2 Observation Time Required to Produce a Background Event Rate of 10^{-6} per Second vs Background Count Rate for $M_V = 6$ Target.....	63
6.3 Background Event Rate vs CCD Frame Integration Time for Various Background Intensities.....	65
6.4 CCD Pixel Readout Frequency and Buffer Memory Size vs Number of CCD Columns (N_x).....	67
6.5 Background Event Rate vs Number of Columns in the Array for Various Background Intensities.....	68

LIST OF FIGURES (Cont.)

<u>Figure</u>		<u>Page</u>
6.6	Background Event Rate vs Target Intensity for Various Background Intensities.....	70
6.7	Limiting Target Intensity vs Background Intensity for Observation Times of 30 Sec. and 60 Sec.....	71
6.8	Limiting Target Intensity vs Solar Angle for Observation Times of 30 Sec. and 60 Sec.....	74

LIST OF TABLES

<u>Table</u>	<u>Page</u>
4.1 Calculated expressions for the peak signals produced by point and square spots crossing CCD 202 and contiguous CCD arrays.....	24

1.0 INTRODUCTION

The Intensified Charge Coupled Device (ICCD) has been identified as a very attractive detector for space applications due to its extremely high sensitivity, small size, ruggedness, low power requirements, absence of lag and suitability for use with a digital data processing system.

The ICCD utilizes a CCD array to detect electrons which are emitted from a photocathode, accelerated by an electric field and imaged onto the CCD which is inside the vacuum tube. Actual measurements⁽²⁾ with an ICCD demonstrated single photoelectron detection with a high signal-to-noise ratio. However, prolonged exposure of the CCD to electrons from the front side of the array produced severe degradation of CCD performance (increased dark signal and decreased sensitivity). The lifetime of the ICCD was identified as a critical issue and is the subject of a separate study.

The purpose of the present study is to evaluate the sensitivity of an ICCD used in space applications. Since the sensitivity is strongly influenced by the data processing techniques used for signal discrimination, candidate techniques have been identified and evaluated using simulated star scanning measurements and photoelectron pulse height distribution data as well as estimated signal and background intensities. For the purpose of this study, the background was assumed to come only from zodiacal light.

It is convenient to divide the detection system into the major functional elements shown in Figure 1.1.

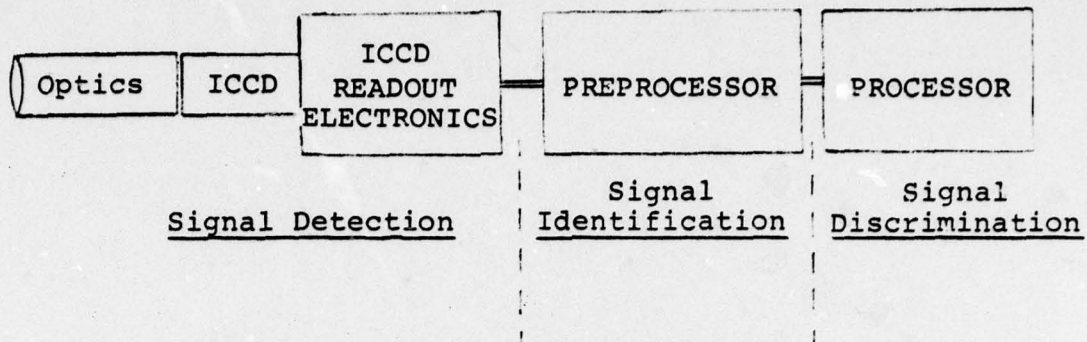


Figure 1.1 Functional Block Diagram of Detection System.

This study is concerned with the performance of the detector and the preprocessor. The specifications for the optical system were assumed to include a focal length of 73mm and an effective collection area of 4.6cm^2 .

The primary function of the preprocessor is that of signal identification and data compression. The large amount of signal and background data from the ICCD is filtered by the preprocessor which passes on to the processor the sensor (x,y) coordinates and intensities of relatively few events which meet the requirements for valid signals. The processor analyzes these events, using additional criteria to identify signals of interest. The processor handles the sensor-to-stellar coordinate transformations, the stellar catalog, ground communications, etc.

The performance of the preprocessor is critical to taking full advantage of the extreme sensitivity of the ICCD which is capable of detecting single photoelectrons with a high signal-to-noise ratio. With such quantum-limited performance, the practical sensitivity is limited by the background intensity. The

background produces signals which, even in the absence of a target, occasionally exceed the detection threshold. In order to minimize these "background events", the preprocessor should integrate the signals for as long a time as possible consistent with the scan rate necessary to cover the required area in the time available.

Integration of the signal without smearing in a scanning CCD can be accomplished in two ways. If the CCD is of the frame transfer type with the signal charge packets being transferred out of the array through the photosites, the array readout clock can be synchronized with the scan motion so that the signal charge in the array moves along at the same rate as the signal spot on the array. Thus, the signal will continue to integrate until the spot moves off of the array. This scheme is known as Time-Delay integration (TDI). For each pixel, only a single readout is made at the end of the integration so the readout noise is minimized. However, not all arrays are operable in the TDI mode. Also, the array readout must be synchronized with the scan motion (or vice versa), and there is a limit to the integrated signal due to saturation being reached in the CCD charge-trapping wells.

The above limitations to the TDI technique can be overcome, at the expense of increased readout noise and more complex external (off-chip) electronics, by adding the signals from successive frames into an external buffer memory. Successive frames are shifted to keep the signal from a single spot in the same place in the buffer memory even though it moves across the

array. This technique, referred to as shift-and-add-integration (SAI) can be used with any array. Since each frame is individually read out, the readout noise is multiplied by the square root of the number of frames added compared to a single readout per integration with the TDI technique. Because the readout noise from an ICCD is a small fraction of a photoelectron, it was neglected in the present study. Using SAI, the frame time can be completely independent of the scan rate since the synchronization is maintained by externally shifting the data before adding it to the external buffer memory. Also, the dynamic range is extended since each frame may contain signals near saturation in the array. If necessary, the data can also be shifted vertically (across the direction of scan) to follow a signal crossing onto different rows in the CCD. In the present study it was assumed that the preprocessor performed SAI for as many frames as necessary for each object to completely cross the array.

After integrating the data, the preprocessor compares each signal with a threshold which is determined so that the minimum anticipated signal, when added to the measured background, will exceed the threshold with the required detection probability. The sensor (x,y) coordinates and intensities of all pixels whose signals exceed the threshold are communicated to the processor.

For a specific target intensity, the performance of the detector-preprocessor system is measured by the "background event rate" (BER), which is the rate at which background signals

(no target) exceed the threshold. In the absence of further processing, the BER would be equal to the false alarm rate for the sensor. In actual practice, however, the processor could reduce the false alarm rate many orders of magnitude below the BER by performing additional correlations.

The sensitivity of the detector-preprocessor system is characterized by the "limiting target intensity" (LTI) which is defined as that target intensity which, for a specified detection probability, produces a BER of 10^{-6} per second (1 event per 11.6 days).

Including specification of the optics, the CCD geometry, frame time, the area to be scanned, the observation time, the visual magnitude of the background, and the visual magnitude and detection probability for the target, a total of fourteen parameters are necessary to specify the conditions for a single scan. In order to make the calculation manageable, the possible combinations (and ranges) of parameters had to be limited.

Two CCD geometries were used, the first being that of the Fairchild CCD 202 which was the array used to generate the scan data. The CCD 202 is an interline transfer device with "dead" columns $22\mu\text{m}$ wide between columns of photosites $18\mu\text{m}$ wide. The number of columns (along the scan direction) was varied from 10 to 100 in the sensitivity calculations.

The second CCD geometry used was that of a contiguous array with the same photosite dimensions and number of photosites (100 x 100) as the CCD 202, but without dead spaces.

The area of sky to be scanned was fixed at 13 degrees by 9 degrees. The remaining five parameters were varied over the ranges indicated below:

<u>Parameter</u>	<u>Range</u>
Observation time	10 to 45 sec.
CCD frame time	2 to 50 msec.
Detection probability	0.98 to 0.999
Target visual magnitude	6 to 10 visual magnitudes
Background Visual magnitude	-3 to 2 visual magnitudes/deg. ²

With the parameters defined as above, the method of determining the sensor sensitivity (LTI) proceeded as follows:

1. The signal and zodiacal light background intensities (photoelectrons/sec) were calculated for a stationary sensor with an S-20 photocathode.
2. The effect of sensor motion (scanning) on the observed signal was calculated and verified by measurement. Shift-and-add integration (SAI) was used to maximize the total signal obtained.
3. The shape of the photoelectron pulse height distribution was calculated using Poisson statistics and verified by comparison with actual CCD photoelectron data.
4. Using the normal (Gaussian) approximation to the signal-plus-background pulse height distribution, the threshold needed to ensure a specified detection probability was calculated.

5. Using the threshold and a Poisson distribution for the background, the number of background-illuminated pixels exceeding the threshold (BER) was calculated.

6. For a range of background intensities, the target intensity (LTI) which resulted in a BER of 10^{-6} per second was determined.

7. The effect of various operating parameters (e.g., CCD frame time, observation time, etc.) on the LTI was investigated to evaluate the sensor performance and determine the optimum conditions.

The analysis assumed that the sensor scan motion is uniform and that the CCD is approximately oriented with the rows of pixels along the scan direction.

2.0 SUMMARY OF RESULTS AND CONCLUSIONS

The sensitivity of the sensor system investigated in this study is summarized in Figure 2.1. The limiting target intensity (LTI) as a function of the angle between the target and the sun (solar angle) is shown for observation times of 30 and 60 sec. These curves were calculated assuming the sensor background was due entirely to zodiacal light with an intensity distribution indicated in Section 3.0 of this report. The absolute responsivity of the ICCD photocathode in terms of photoelectrons per second for a given target (or background) light intensity was taken from the earlier study by Kash and Chang⁽¹⁾.

The extreme sensitivity of the ICCD is apparent from the results shown in Figure 2.1. Even relatively close to the sun, targets as weak as eighth magnitude can be detected. Farther from the sun, the sensitivity increases although the corresponding signals drop to a few photoelectrons per frame at about 35 degrees. Beyond 35 degrees (shown by dashed curves), the sensitivity continues to increase and single photoelectron detection becomes necessary. For these signals, the effect of CCD readout noise may make the present analysis inaccurate, but should not change the basic conclusion that ninth magnitude targets are detectable in 30 sec. and tenth magnitude in 60 sec.

The results shown in Figure 2.1 were calculated for the CCD 202 geometry (100 x 100 pixels) operating at 50 frames per second ($I = 20$ msec). This rate results in an individual pixel rate of about 0.6 MHz which is reasonable in terms of the requirements for signal processing and buffer memory electronics.

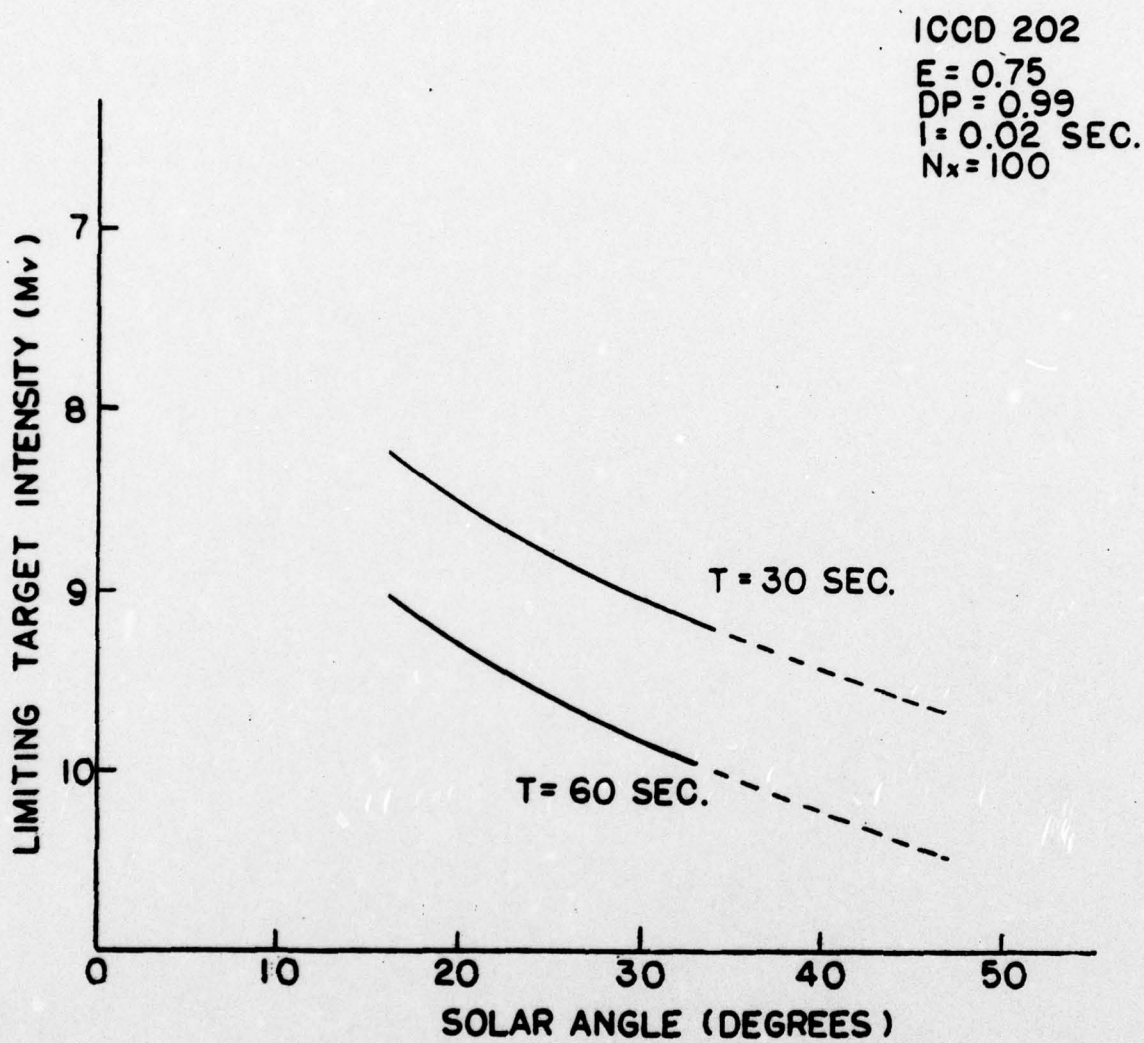


Figure 2.1. Limiting Target Intensity vs Solar Angle for Observation Times of 30 Sec. and 60 Sec.

The buffer memory required for subtraction of the fixed pattern (dark current) from the array output must be the same size (number of words) as the array. The signal integration (SAI) buffer must also be the same size as the array (or slightly larger depending on the processing scheme used). Thus, the total buffer required for a 100 x 100 array is at least 20,000 words.

In the regions of the sky where backgrounds and LTIs are high, the sensitivity of the TWS may be increased by decreasing the CCD frame time. However, high pixel readout rates are undesirable due to the increase in the bulk, weight and power requirements of the signal processing and buffer memory electronics as the operational speed increases. The frame time may be decreased without increasing the pixel rate if the number of pixels are decreased. A limited investigation of the tradeoff between number of pixels along the scan direction (N_x) and the frame time (I) seemed to indicate that the decrease in performance with a decrease in N_x was not as great as the increase in performance obtained by a proportionate decrease in frame time. Thus, it may be advantageous to decrease N_x (and the buffer memory required) and I , perhaps by a factor of two (i.e., a 50 x 100 pixel array operating at a 10 msec frame time).

Over most of the parameter range studied, the CCD 202 geometry was slightly superior to the contiguous array. This situation reversed at very low frame times (about 5 msec) where the contiguous array showed significantly better performance. For a contiguous array the optimum number of columns may be re-

duced even further than for the CCD 202 perhaps to a 20 column array operating at $I = 4$ msec.

The sensitivity (LTI) of the TWS is strongly enhanced by using signal integration (SAI) and the results in Figure 2.1 were calculated assuming its use. Sample calculations for single-frame detection at an observation time of 30 sec. indicated a loss in sensitivity of approximately 1.7 stellar magnitudes.

The LTI was not very sensitive to the detection probability. Calculations were performed for a DP of 0.999 and the loss of sensitivity compared to the DP = 0.99 results was only 0.1 stellar magnitudes. Thus, very reliable detection is possible while maintaining the high sensitivity.

The increase in LTI with an increase in observation time is shown in Figure 2.1 by the difference between the $T = 30$ sec and $T = 60$ sec results. This doubling of the observation time resulted in an increase in sensitivity of about 0.8 stellar magnitudes. Presumably, even higher sensitivity would be possible at longer observation times.

For the calculations presented in Figure 2.1, the target spot intensity was derated by 25% ($E = 0.75$) to allow for vertical misalignment between the spot and the rows of pixels. This value of E represents an average of the minimum value of 0.5 for the spot falling midway between two pixels and the maximum of 1.0 with the spot centered on a pixel. Using an array with staggered pixels (i.e., alternate columns offset vertically by $1/2$ the pixel height), would ensure an E of about 0.75 for any

spot alignment. Even without staggered pixels, an angular misalignment of the array or significant sensor motion normal to the scan direction would cause the spot to move from one row of pixels to another and therefore ensure an average value $E = 0.75$. In this case, however, as the spot moves from one row to another, a vertical shift must be used in the shift-and-add integration procedure to maintain synchronism with the target spot.

An alternate method of processing the CCD data that would make $E = 1$ would be to sum adjacent pairs of rows of pixels. Rows 1 and 2 would be summed and labeled row 1, rows 2 and 3 would be summed for row 2, etc. The entire spot (diameter less than one pixel height) would always appear in at least one summed pair. The increase in the signal compared to the $E = 0.75$ assumption is equivalent to a sensitivity increase of 0.31 stellar magnitudes. However, summing adjacent rows would cause the background to double. Doubling the background causes a decrease in sensitivity of about 0.35 stellar magnitudes. The conclusion is that no increase in sensitivity would result from summing adjacent rows and using the technique would definitely not be worth the extra complexity introduced into the signal processing electronics.

3.0 TARGET AND BACKGROUND INTENSITIES

3.1 Target Intensity

The purpose of the present study is to evaluate the sensitivity of the ICCD under a variety of operating conditions. For this purpose, the target was characterized by its intensity in visual magnitudes (m_v). In order to provide realistic results, visual magnitudes between +5 and +10 were evaluated.

The electron signal intensity on the array within the ICCD depends on the characteristics of the optics and the ICCD photocathode. The baffled telescope assumed for use in the system has a focal length of 73.1 mm and an effective light-collection aperture area of 4.62 sq. cm.

The ICCD photocathode sensitivity was taken from the report by Kash and Chang. Using their normalization factor for an S-20 photocathode, we can calculate the number of photoelectrons/sec from a target with apparent visual magnitude m_v :

$$n_o = 4.1 \times 10^9 \cdot A \cdot 10^{-m_v/2.5} \text{ pe/sec} \quad (3.1)$$

where A is the effective telescope aperture area (m^2). A seventh magnitude target and the candidate telescope yields a signal of 3000 photoelectrons per second.

The spot size was taken to be about 20 μ m in diameter. It will be shown in Section 5.0 of this report that the results of this study are not very sensitive to spot size as long as it is smaller than about 25 μ m.

3.2 Background Intensity

The major source of diffuse sky background is the zodiacal light. Surrounding the sun is a cloud of dust particles whose spacial density decreases with distance from the sun. Concentrated towards the plane of the ecliptic, the dust cloud scatters sunlight producing a bright sky background known as the zodiacal light. Brightness of the zodiacal light as a function of solar elongation angle and ecliptic latitude is given by Allen⁽³⁾ and the data for Figure 3.1 were taken from there. Figure 3.1 shows intensity (apparent visual magnitude per square degree) of the zodiacal light as a function of solar elongation angle for ecliptic latitudes of 0 and 30 degrees. For an apparent visual magnitude per square degree of M_b , the background count rate per pixel per second in the ICCD is given by:

$$n_b = 4.1 \times 10^9 \cdot A \cdot \Delta\phi \cdot \Delta\theta \cdot 10^{-M_b/2.5} \quad (3.2)$$

where A is the telescope effective aperture (m^2) and $\Delta\phi$ and $\Delta\theta$ are the pixel angular acceptances (.0141 and .0235 degrees respectively).

For the CCD 202 geometry (18 x 30 μ m pixels) and the candidate telescope, the background count rate per pixel per second was calculated and is shown in Figure 3.2. The 0 degree ecliptic latitude was used for calculating the background count rate to ensure a conservative estimate of sensor performance.

The calculated direct zodiacal light background count rate at 10 degrees from the sun is about 2000 photoelectrons per second. At this small angle the actual background count rate will exceed that predicted by the curve in Figure 3.2 due to other effects such as scattering from the telescope baffles. No such effects were considered in this study. Background count rates above 2000 counts/sec were occasionally considered to investigate the limits of sensor performance. However, no reliable correlation of count rate vs solar angle was attempted at small angles.

Estimates of the sky background produced by integrated starlight (unresolved stars) were performed and were found to be relatively insignificant compared to the zodiacal light. The maximum value of the integrated starlight background occurs in the plane of the ecliptic and has an apparent visual magnitude of about 3.57 per square degree. This background will be significant only for solar angles larger than 40 degrees, and so was neglected in this study.

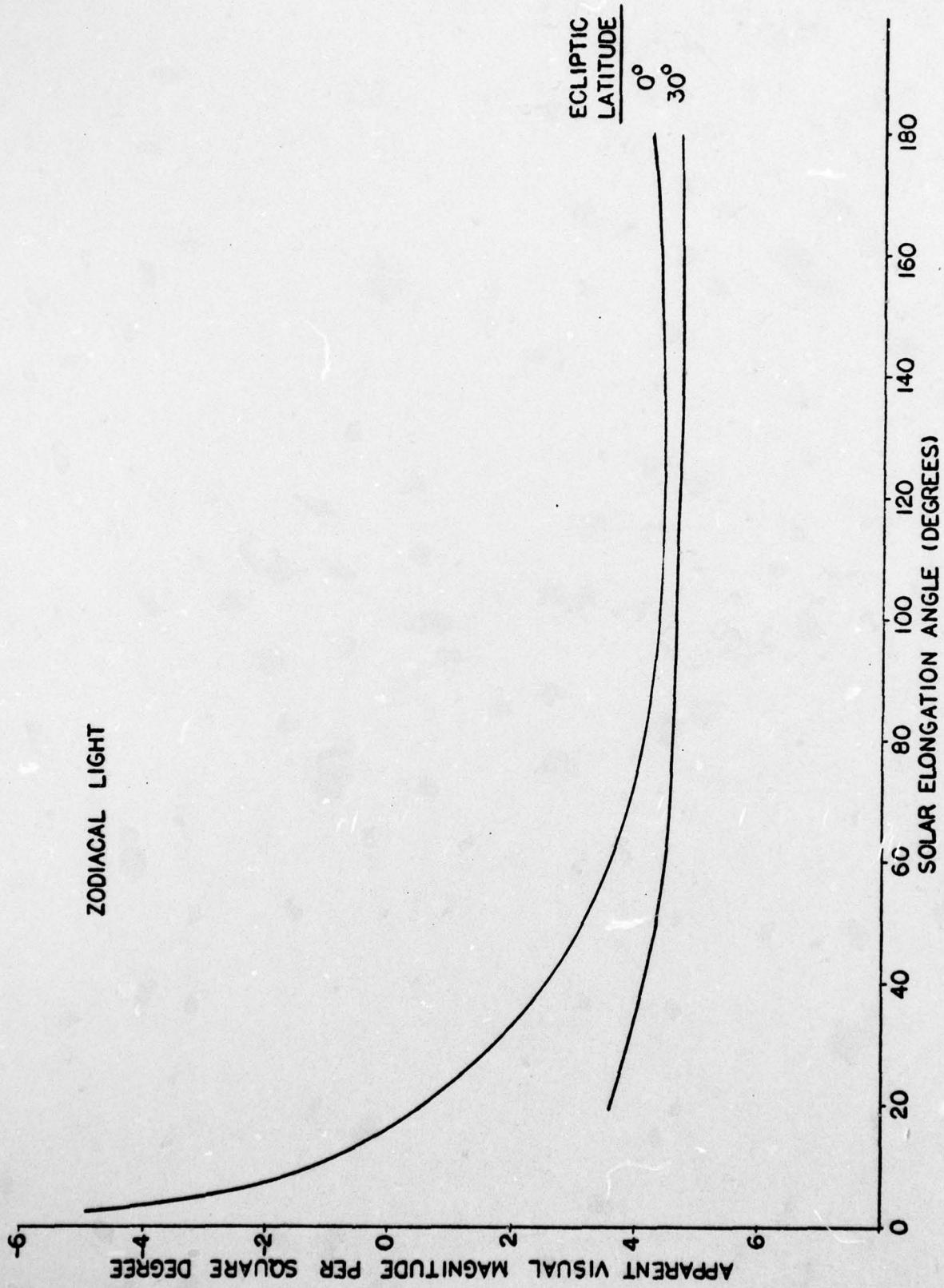


Figure 3.1. Zodiacal Light Intensity vs Solar Elongation Angle

ZODIACAL LIGHT BACKGROUND COUNT RATE
CCD AND CANDIDATE TELESCOPE

$\Delta X = 18 \mu\text{m}$
 $\Delta Y = 30 \mu\text{m}$

$f\lambda = 73.1 \text{ m}$
 $f\star = 20$
 $T\# = 3.0$

$\Delta\theta = 0.0141 \text{ DEG}$
 $\Delta\theta = 0.0235 \text{ DEG}$

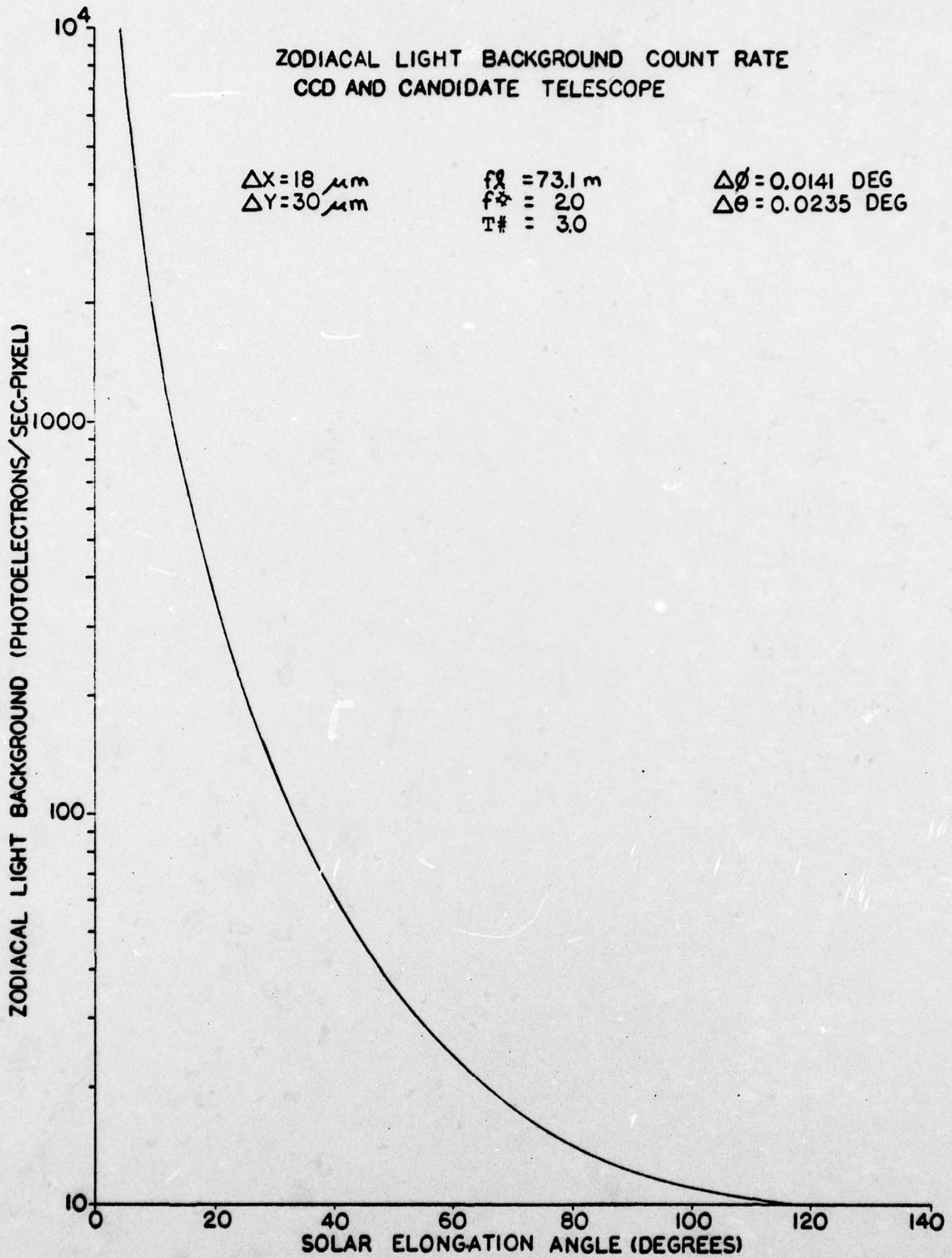


Figure 3.2. Zodiacal Light Background Count Rate per Pixel vs Solar Elongation Angle

4.0 SENSITIVITY ANALYSIS

4.1 Scanning Geometry and Rate

In order to observe an area of sky greater than the sensor field of view (FOV), the sensor must be scanned. Even if the sensor FOV covers the required observation area, some sensor motion may be desirable due to the possibility of array defects or dead areas (e.g., the shift-register areas on an interline transfer array) obscuring a target. To minimize the background, it is desirable to make the individual pixel FOV as small as possible consistent with the target spot size. However, a reduction in sensor field-of-view increases the scan speed required to cover a given area in a given time.

In the present analysis it is assumed that the sensor has a total FOV of θ degrees (in the scanning or x-direction) by θ degrees (y-direction) with the corresponding numbers of pixels N_x and N_y . The sensor scans an area θ_s (x-direction) by θ_s in a back-and-forth sweeping pattern illustrated in Figure 4.1. For maximum signal, it is desirable to have each point in the scanned area completely cross the array. Therefore, the sensor angular travel per x-scan is $\theta_s + \theta$ and the number of x-scans is θ_s/θ . The total angular travel in the y-direction is approximately (not allowing for overlapping coverage) $\theta_s - \theta$. The total angular travel in a complete scan is $(\theta_s + \theta) \theta_s/\theta + (\theta_s - \theta)$. Assuming a uniform scanning speed, S (degrees/sec), over an observation time T (sec) we get:

$$S = [(\theta_s + \theta) \theta_s/\theta + \theta_s - \theta]/T \text{ degrees/sec} \quad (4.1)$$

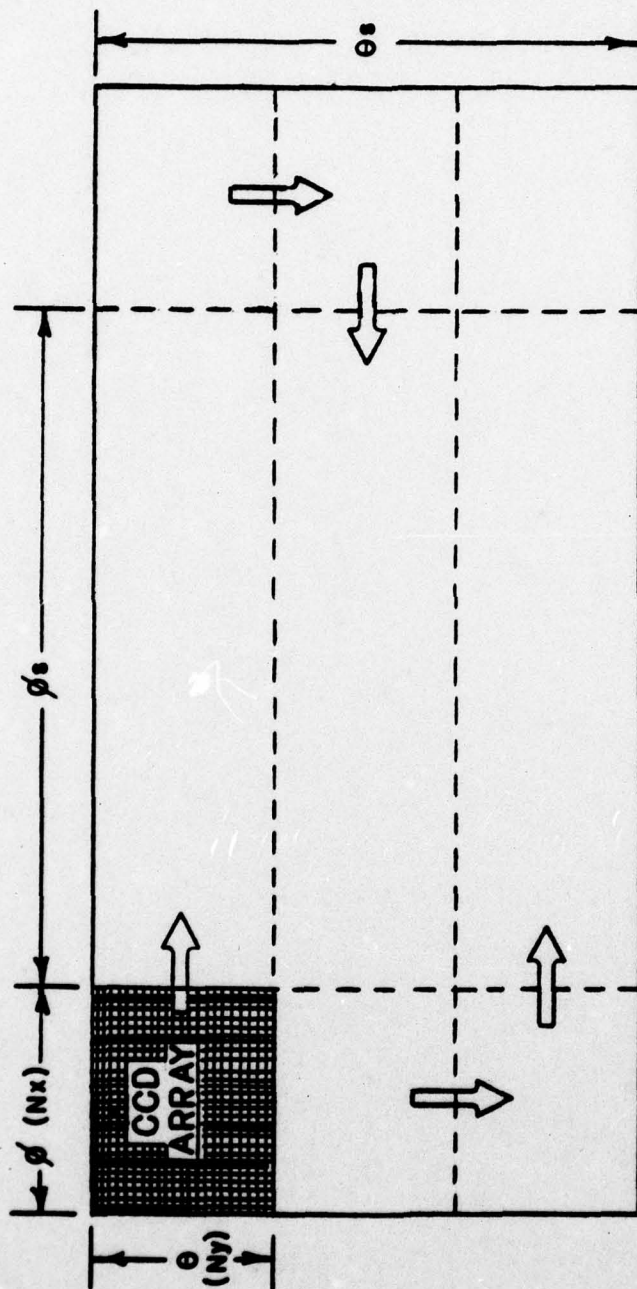


Figure 4.1. ICCD Scanning Geometry

At a speed of S degrees/sec, the target spot crosses the array (N_x pixels) in θ/S seconds and so the spot velocity in pixels crossed per second is $S \cdot N_x / \theta$. It will be seen in the next section that for the purpose of characterizing the effect of sensor motion on the signal, it is convenient to express the spot velocity across the array as the number of pixels crossed during one CCD frame (or integration) time. For a frame time of I (sec), the spot velocity, P (pixels/frame), is given by:

$$P = \frac{S \cdot I \cdot N_x}{\theta} \quad \text{pixels/frame} \quad (4.2)$$

4.2 Effect of Sensor Motion on Target Signal

In this section, the signals produced by a spot crossing the CCD array will be calculated. Previous studies indicated a realistic spot diameter approximately equal to the width of a pixel. In the present analysis this situation was represented by using a square spot with sides equal in length to the active width (in the x-direction) of a pixel and uniform intensity over the spot. In order to see the effect of spot size on the signal, the analysis was also carried out for a point spot. Two array geometries were considered: the Fairchild CCD 202 (interline transfer) which was used to generate data, and a contiguous geometry with pixel width equal to the sensitive pixel width on the CCD 202 but with no dead spaces.

The upper curve in Figure 4.2 shows the instantaneous count rate, $n(t)$, on a pixel as a function of time while the spot is crossing the pixel. The velocity, v , of the spot across the array can be expressed as:

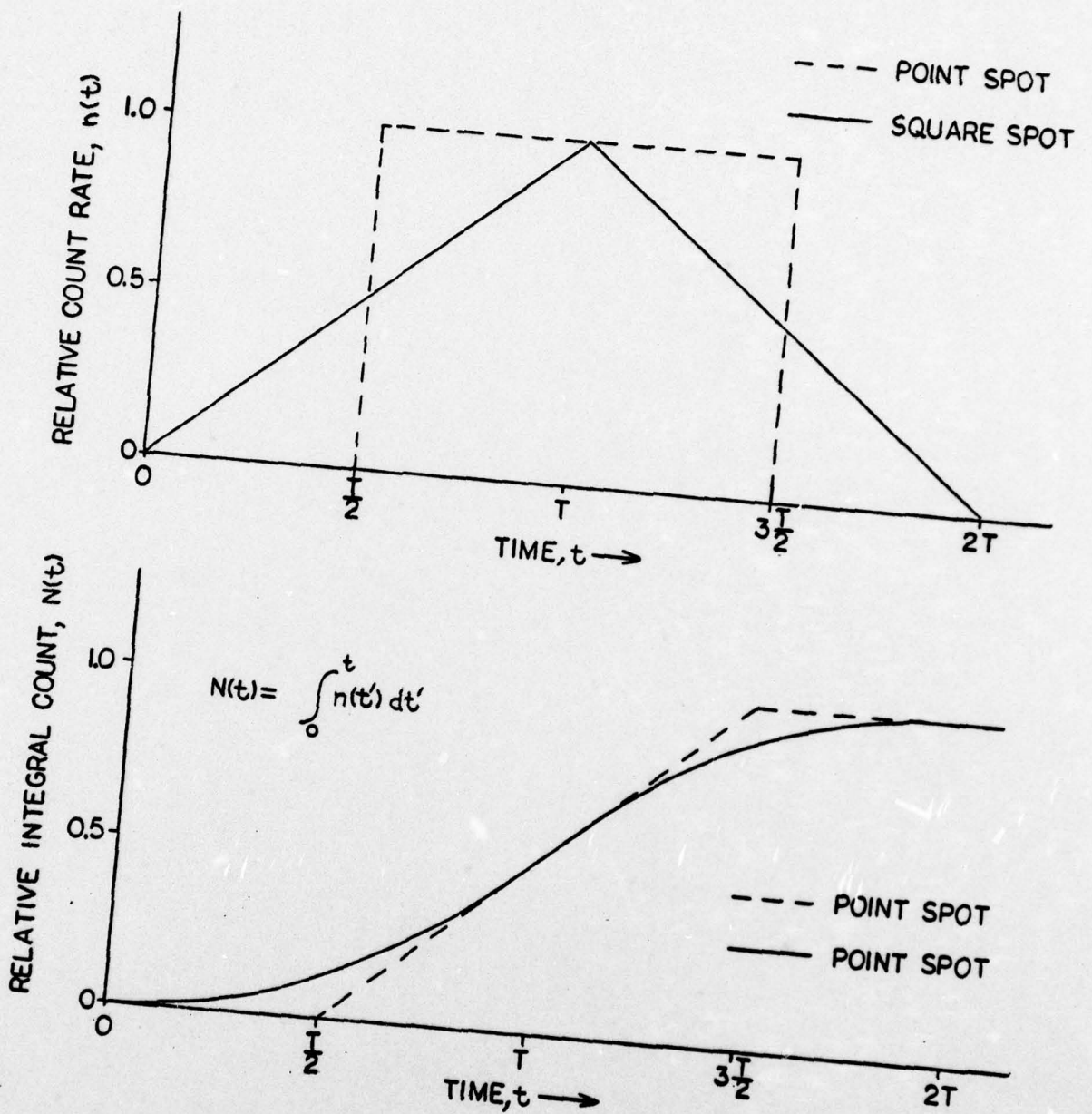


Figure 4.2. Relative Count Rate and Integrated Count as a Function of Time as a Moving Spot Crosses a CCD Pixel

$$v = \frac{P(a+d)}{I}$$

where P is the velocity in pixels/frame, a and d are the widths of the photosensitive and dead regions of the pixel, and I is the frame time. The time, T', for the centroid of the spot to travel across the pixel live region is given by:

$$T' = \frac{a}{v} = \frac{a}{(a+d)} \cdot \frac{I}{P} \quad (4.3)$$

For the CCD 202 geometry, a = 18 μ m and d = 22 μ m yielding the geometrical factor, a/(a+d), of 0.45. For a contiguous array, d = 0 and the geometrical factor is unity. Therefore, Equation 4.3 gives:

$$T' = 0.45 I/P \quad (\text{CCD 202})$$

and

$$T' = I/P \quad (\text{Contiguous})$$

The integrated signal as a function of time is shown in the lower curve in Figure 4.2. The total integrated signal as the spot completely crosses the array (i.e., the area under the count rate vs time curve) is the same for the square and point spots. This total integrated signal (S_{int}) is easily obtained from Figure 4.2 as:

$$S_{int} = n_o T' \quad (4.4)$$

where n_o is the peak instantaneous count rate (photoelectrons/sec) in the entire spot. Using Equation 4.3, we obtain:

$$S_{int} = 0.45 n_o I/P \quad (\text{CCD 202}) \quad (4.5)$$

$$S_{int} = n_o I/P \quad (\text{Contiguous}) \quad (4.6)$$

The data will be compared with Equation 4.5 in Section 5.0.

In the actual operation of the CCD array, the signal obtained from a pixel is integrated for the frame time, I. The beginning and ending of the frame time is in general completely random compared to the time during which the spot crosses the array. As the spot crosses the entire array, the signal will vary as the phase of the frame time relative to the spot position changes. When the spot is in phase with the peak count rate the signal will reach a maximum. This peak signal can be calculated. Referring to Figure 4.2, the peak signal will occur when the frame integration time is centered on the peak count rate at time T. The peak signal is given by:

$$N_p = \int_{T'-I/2}^{T'+I/2} n(t') dt' \quad (4.7)$$

The results for the CCD 202 and the contiguous CCD, using both the point and square spots are presented in Table 4.1. These results will be compared to the data in the next section.

At low scanning speeds (P less than about 2 pixels per frame) the estimation of sensor performance based on detection of peak signals is difficult due to the sensitivity of the signal to the relative phases of the CCD integration time and the position of the spot. In addition, detection at or near the peak signals does not take advantage of the signal outside of the region of the peak which may be substantial when integrated across the

ICCD ARRAY GEOMETRY	SCAN SPEED P (PIXELS/FRAME)	EXPRESSIONS FOR PEAK SIGNALS	
		POINT SPOT	SQUARE SPOT
CCD 202	$P \leq 0.45$	$n_o \cdot I$	$n_o \cdot I(1 - 0.56P)$
CCD 202	$0.45 < P \leq 0.9$	$0.45 n_o \cdot I/P$	$n_o \cdot I(1 - 0.56P)$
CCD 202	$P > 0.9$	$0.45 n_o \cdot I/P$	$0.45 n_o \cdot I/P$
Contiguous	$P \leq 1$	$n_o \cdot I$	$n_o \cdot I(1 - P/4)$
Contiguous	$1 < P \leq 2$	$n_o \cdot I/P$	$n_o \cdot I(1 - P/4)$
Contiguous	$P > 2$	$n_o \cdot I/P$	$n_o \cdot I/P$

Table 4.1. Calculated expressions for the peak signals produced by point and square spots crossing CCD 202 and contiguous CCD arrays.

array. For these reasons, the detection scheme used here is based on integration of the signal as the spot moves across the array. This may be accomplished using Time Delay Integration (TDI) or Shift-and-Add Integration (SAI) as explained in Section 1.0 and illustrated with data in Section 5.0.

To determine the total integrated signal as the spot crosses the array, the average signal per frame for the appropriate scan speed is obtained and then multiplied by the number of frames during which the spot is on the array. This separation allows the effects of scan speed and number of pixels (N_x) to be separately evaluated.

As the spot crosses the array, the largest signal in any one frame will move from one pixel to another. The TDI or SAI technique is used to shift from pixel to pixel in such a way as to integrate the largest signal in each frame. Therefore, the minimum signal of interest occurs when the spot is midway between two pixels, and the signals of interest from the Nth pixel occur between the time that the spot is centered between the N-1 and Nth pixels and the time it is centered between the N+1 and Nth pixels. This is illustrated in Figure 4.3. During this time interval the spot travels a distance equal to the center-to-center spacing of the pixels ($a + d$) in the time I/P . The average signal (\bar{N}_s) is given by:

$$\bar{N}_s = P/I \int_{T'-I/2P}^{T'+I/2P} dy \int_{\gamma-I/2}^{\gamma+I/2} n_o(t') dt' \quad (4.8)$$

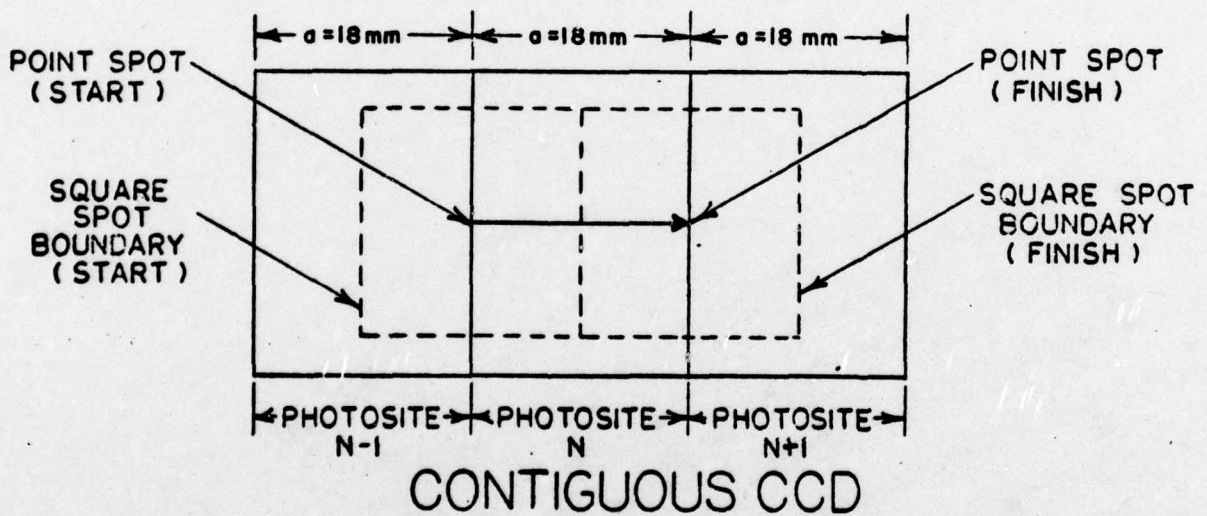
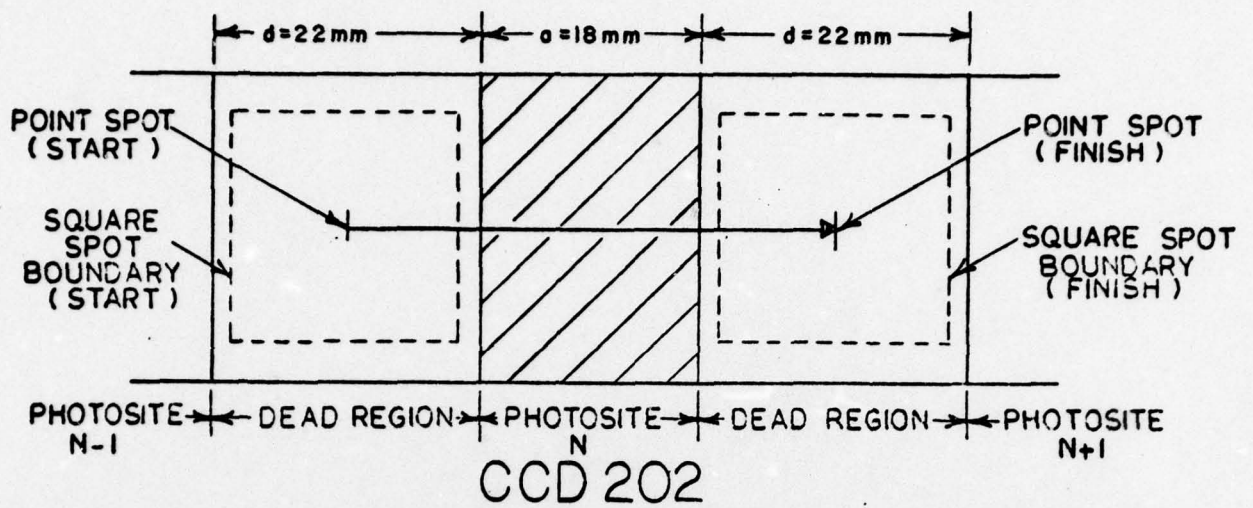


Figure 4.3. Geometry Used to Calculate the Average Signal per Frame as Spot Crosses the CCD Array.

Due to the discontinuous nature of the derivatives of the functions involved (see Figure 4.2) a closed-form solution to Equation 4.8 is possible only for certain cases.

For low scanning speeds ($P < 1$), the average signal in a contiguous CCD can be obtained in closed form. For the point spot, the result is

$$\bar{N}_s = n_o I (1-P/4) \quad (4.9)$$

and for the square spot

$$\bar{N}_s = 0.75 n_o I \left(1 - \frac{P^2}{9}\right). \quad (4.10)$$

At high scanning speeds (P greater than about 2.5 for the contiguous array and about 1.5 for the CCD 202) the average signals become equal to the peak signals given in Table 4.1:

$$\bar{N}_s = 0.45 n_o I/P \quad (\text{CCD 202}) \quad (4.11)$$

$$\bar{N}_s = n_o I/P \quad (\text{Contiguous}) \quad (4.12)$$

Suitable approximations to the exact value of \bar{N}_s for all values of P have been obtained by numerical integration and comparisons with the scanning data will be presented in Section 5.0.

The average signal per pixel per frame was multiplied by a factor, E , to account for the fact that the entire spot may not cross a particular pixel due to its vertical (y) position. Since the spot was no larger than one pixel and the pixels are contiguous in the y direction, E will have a value between 0.5 and 1.0. To provide a conservative estimate of performance, E was usually taken to be 0.5. The use of a constant E implies

that the spot travels along a row of pixels in perfect alignment or that a correction is made to the SAI procedure (i.e., a vertical shift) when the spot crosses from one row to the next.

4.3 Background Event Rate Calculation

The performance of the ICCD sensor is expressed by the Background Event Rate (BER) which is the rate at which signals from pixels, illuminated only by the background, exceed the detection threshold. This BER was determined from the average signal and background as follows. The number of frames (N_f) during which the spot is on the CCD is given by:

$$N_f = N_x/P \quad (4.13)$$

and the average signal per frame is (from Section 4.2) $\bar{N}_s \cdot E$. The background count rate (see Section 3.2) is n_b photoelectrons/sec of which \bar{N}_b will be counted during each frame time ($\bar{N}_b = n_b \cdot I$). Thus, in N_f frames the total signal will be $N_f \cdot \bar{N}_s \cdot E$ and the background will be $N_f \cdot \bar{N}_b$. The total count will be given by:

$$N_T = N_s + N_b = N_f (\bar{N}_s \cdot E + \bar{N}_b) \quad (4.14)$$

The detection threshold is determined from the total count and the required detection probability (DP). Both background and signal are random variables with Poisson distributions. For large means, the Poisson distribution is well approximated by a Gaussian distribution. For example, for a Poisson distribution with a mean of 20, a DP of 0.95 requires a threshold of 12.9. The corresponding threshold calculated using a normal (Gaussian) distribution gives a threshold value of 12.7. Most of the signals of interest here yield considerably more than 20 counts

(mean) and therefore the Gaussian distribution can be used to determine the threshold.

For a total number of counts N_T , the threshold value (THR) is given by

$$\text{THR} = N_T - F \sqrt{N_T} \quad (4.15)$$

where F is the number of standard deviations from the mean required to produce a given DP. Values of F used range from 2.326 for a DP of 0.990 to 3.08 for a DP of 0.999.

Figure 4.4 illustrates the relationship between the signal, background, threshold, DP, and Background Event Probability (BEP). Once the threshold has been established, as explained above, the BEP is calculated from a Poisson distribution with a mean of N_b . By analogy with the DP calculations, the difference between the mean, N_b , and the threshold, THR, is expressed in units of $\sqrt{N_b}$:

$$Q = \frac{\text{THR} - N_b}{\sqrt{N_b}} \quad (4.16)$$

However, in this case a Gaussian distribution is not used since it would underestimate the BEP as shown in Figure 4.5. This figure shows the BEP vs Q for a Gaussian distribution as well as Poisson distributions with mean values (M) of 100 and 196. For values of N_b greater than 196, the curve for $M = 196$ was used to provide a conservative estimate of the BEP.

Finally, the BER was determined by multiplying the BEP by the rate at which pixels are processed from the array:

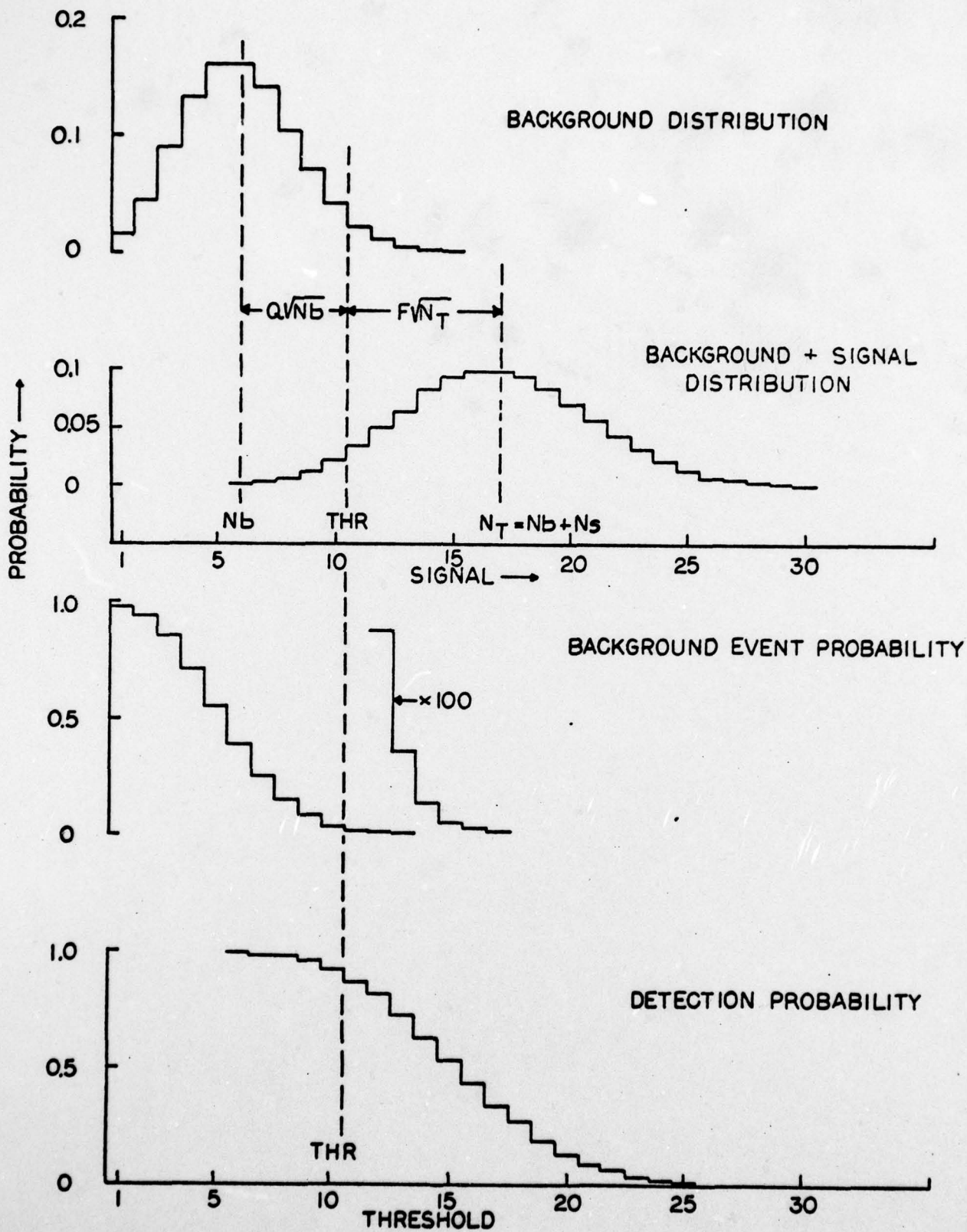


Figure 4.4. Relationship Between Signal, Background, Detection Probability and Background Event Probability

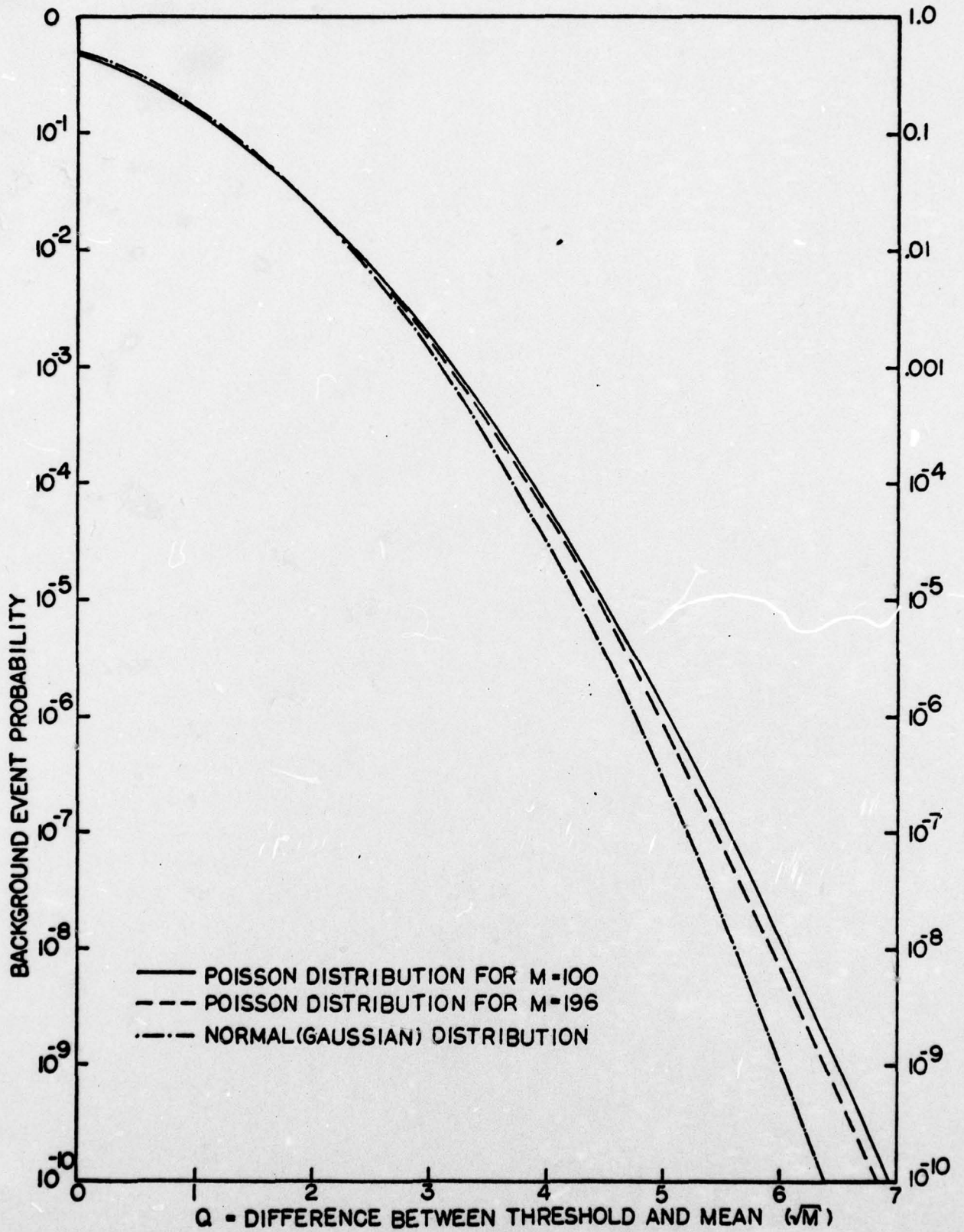


Figure 4.5. Background Event Probability vs Q for Normal and Poisson Distribution

$$\text{BER} = \text{BEP} \frac{N_x \cdot N_y}{N_f \cdot I} \quad (4.17)$$

The results of sample calculations using this analysis will be presented in Section 6.0.

5.0 SCANNING MEASUREMENTS

Star scanning measurements for an ICCD detector were simulated in the laboratory by separately measuring the effect of sensor motion on a scanned visible-light image and the signal distributions of stationary electron-induced images. The scanning measurements were analyzed to obtain the relative signal as a function of scan speed (Sections 5.1 through 5.5) and the signal distribution measurements verified the Poisson shape of the distribution for mean signals of more than a few photoelectrons (Section 5.6). The experimental results were combined analytically (see Section 6.0) to predict the ICCD performance under various operating conditions.

5.1 Scanning Apparatus

Figure 5.1 shows a diagram of the apparatus used to obtain the scanning measurements. The light source, a tungsten-halogen lamp behind a .010 inch pinhole, was located approximately 15 meters from the rotating mirror used to scan the spot across the CCD array. The array used for these measurements was a Fairchild CCD 202 which is an interline transfer device with 100 x 100 pixels. The photosites are arranged in contiguous columns 18 μ m wide separated by light-insensitive columns 22 μ m wide containing the vertical shift registers. The spot was scanned across the columns along one row of pixels.

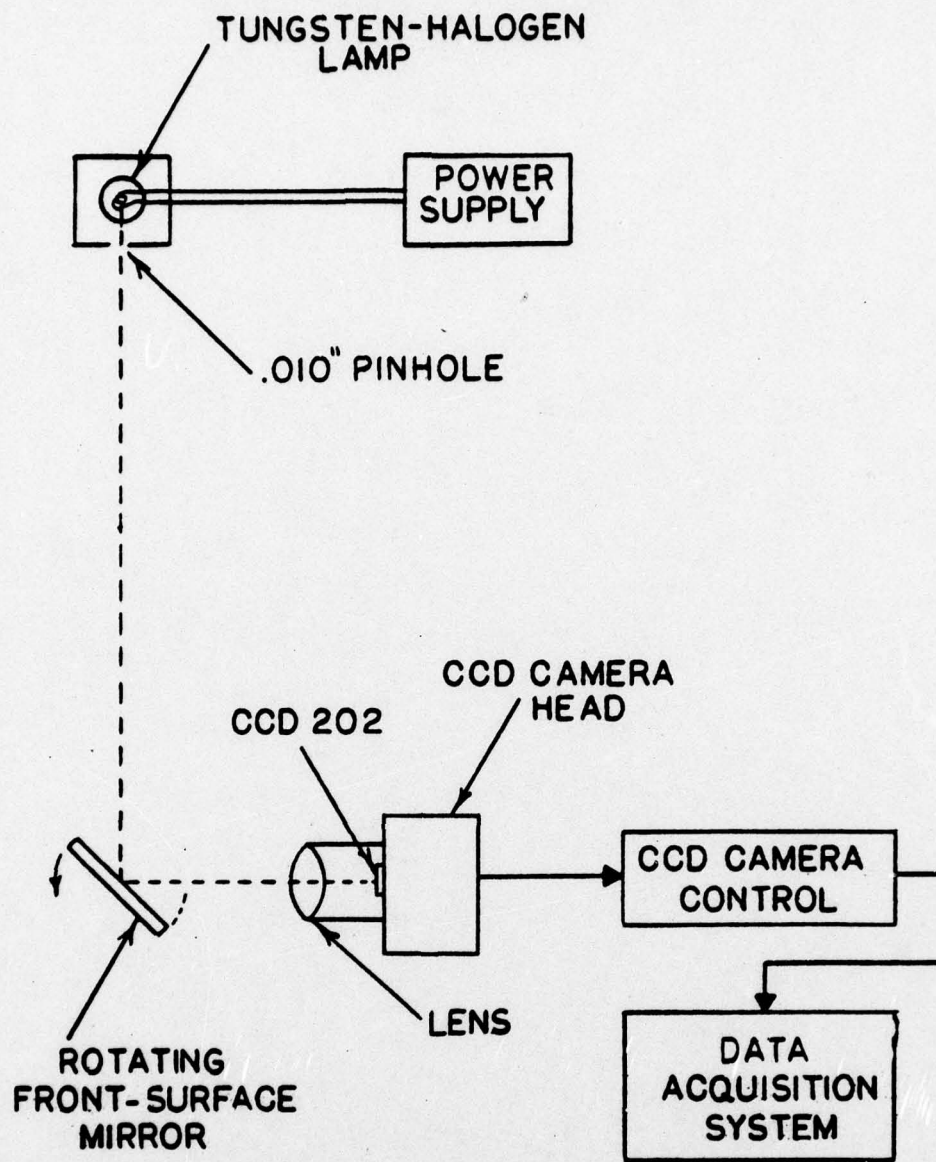


Figure 5.1. Apparatus Used to Obtain Scanning Measurements

5.2 Scanning Data

Using the apparatus described above, a spot of light was focused onto the CCD array. The total diameter of the spot was estimated to be about $25\mu\text{m}$ since it almost disappeared (i.e., the signal dropped to a few percent of the peak value) when the spot crossed the $22\mu\text{m}$ wide dead region between pixels. The intensity distribution was such that the signals produced were between those calculated for a point spot and an $18\mu\text{m}$ square spot with uniform intensity. Comparisons between the data and calculations will be presented later in this section.

The digitized signals from 30 pixels in one row of the CCD were recorded as the light spot crossed them. The array was carefully aligned with the scan direction and no systematic signal variation (indicative of misalignment) was observed. The CCD was operated at a frame rate of 86 frames per second corresponding to a frame integration time of 11.6msec. The rotation rate of the mirror was varied so that scan rates across the array of between 0.15 and 2.44 pixels per frame were obtained. Therefore, the number of frames necessary for the spot to cross all 30 pixels varied between 12 and 200.

Figures 5.2 through 5.6 show the relative signal at the various scan speeds. In each figure, the curves on the left show the signal as a function of time (measured in CCD frame integration times) for several pixels in the row. The time distribution for a single pixel is quite wide at low speeds, indicating that many frames are required for the spot to cross each pixel. Also, at low speeds there are times when the spot almost

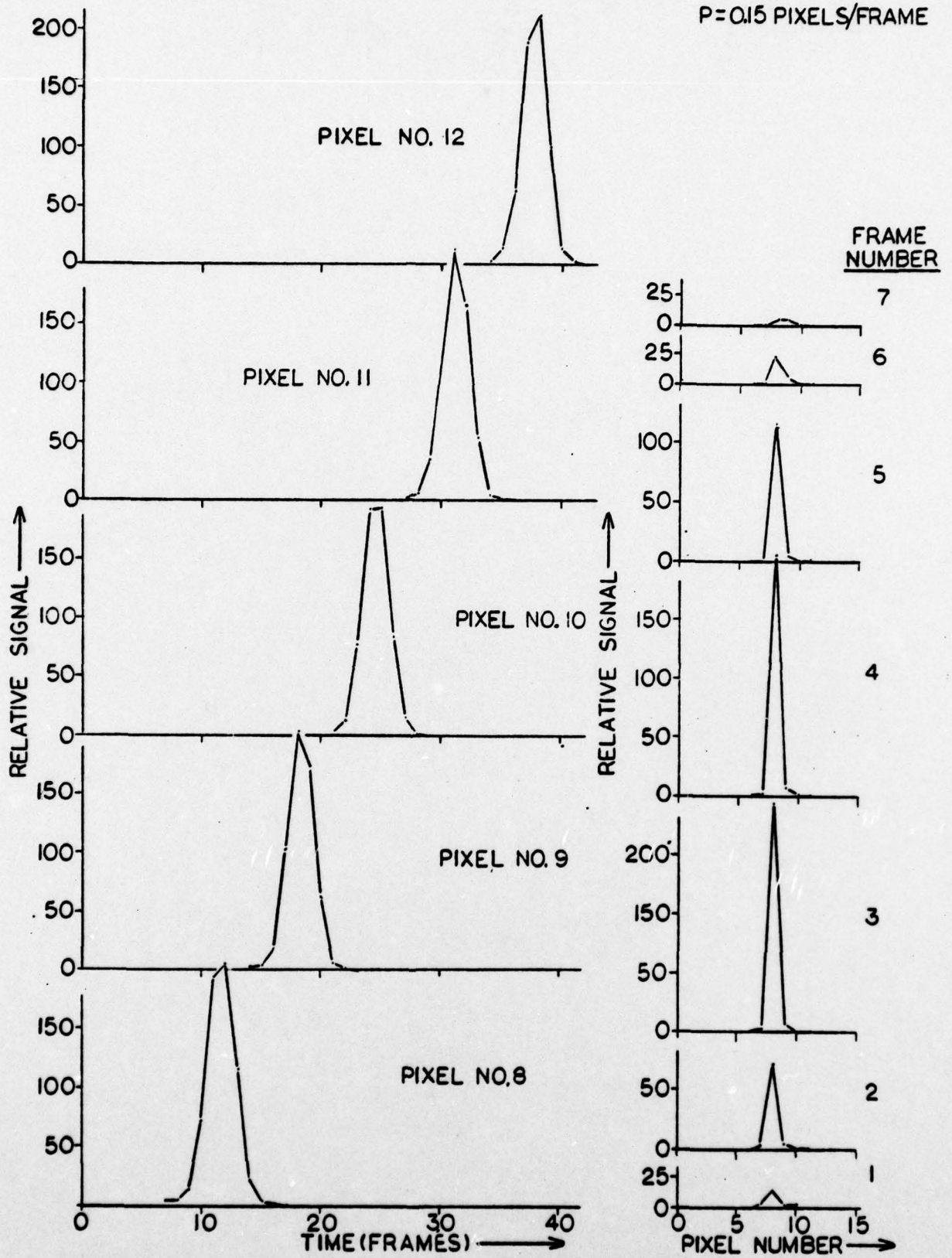


Figure 5.2. Scan Data at a Scan Speed of 0.15 Pixels/Frame

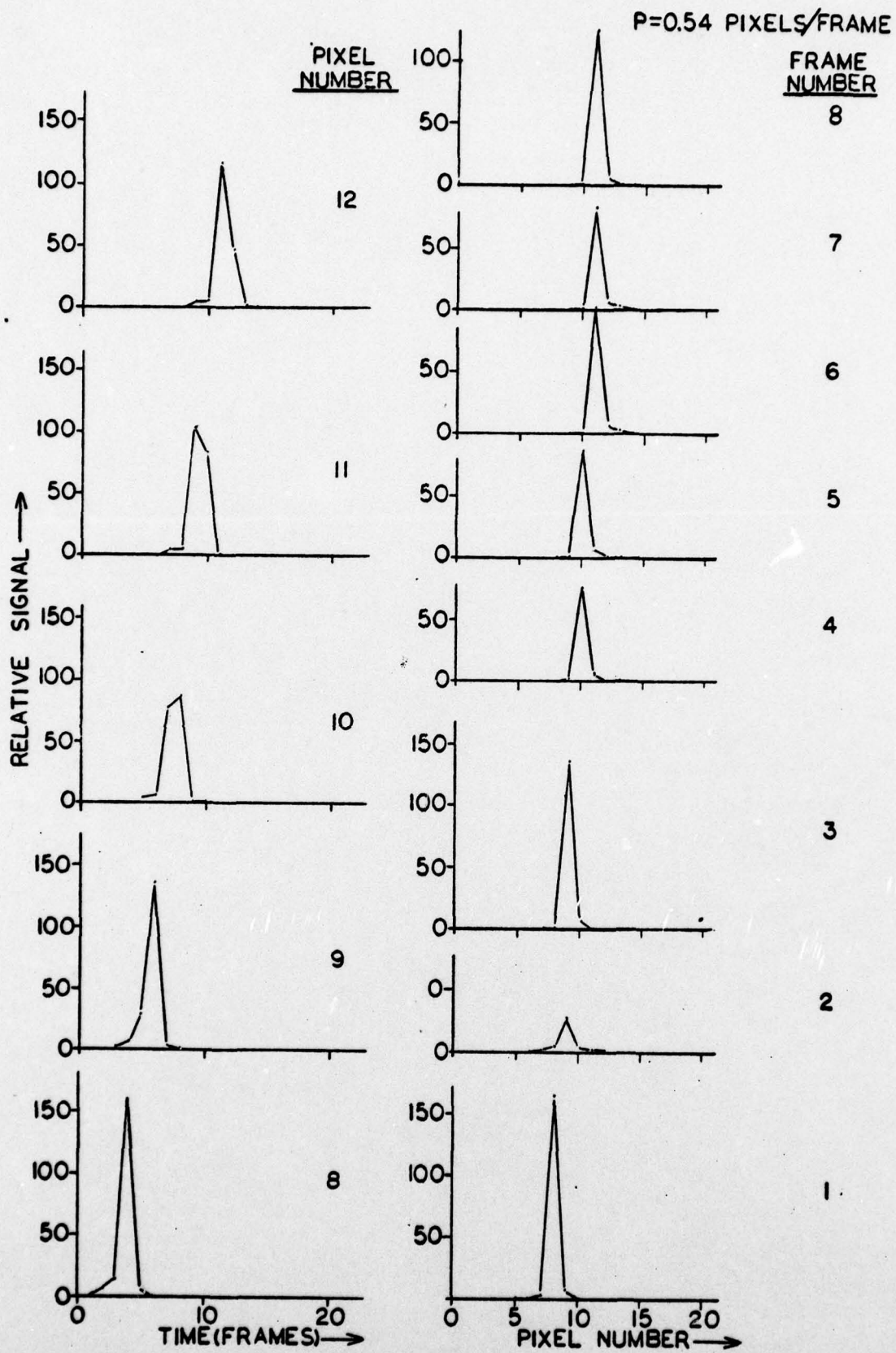


Figure 5.3. Scan Data at a Scan Speed of 0.54 Pixels/Frame

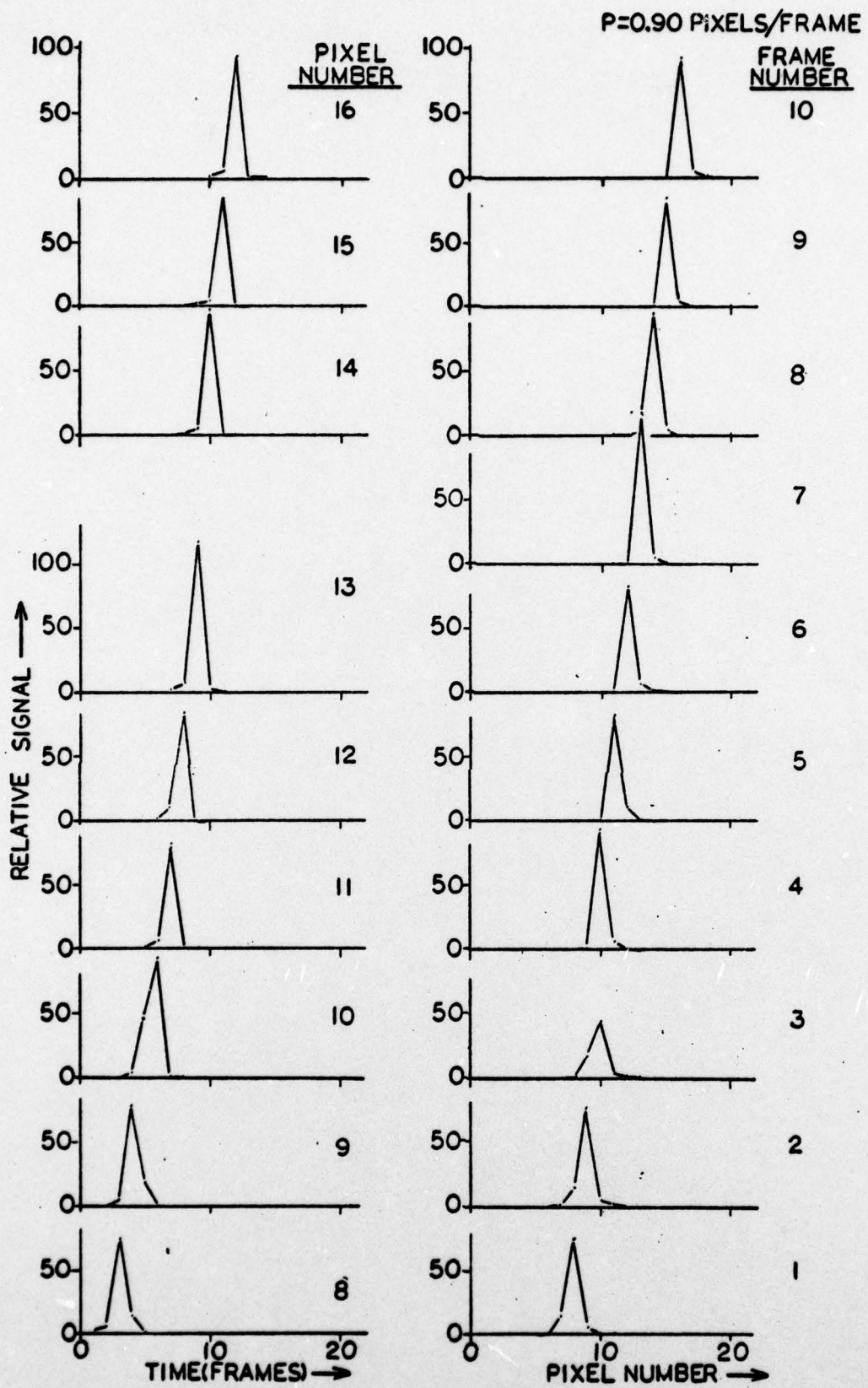


Figure 5.4. Scan Data at a Scan Speed of 0.9 Pixels/Frame

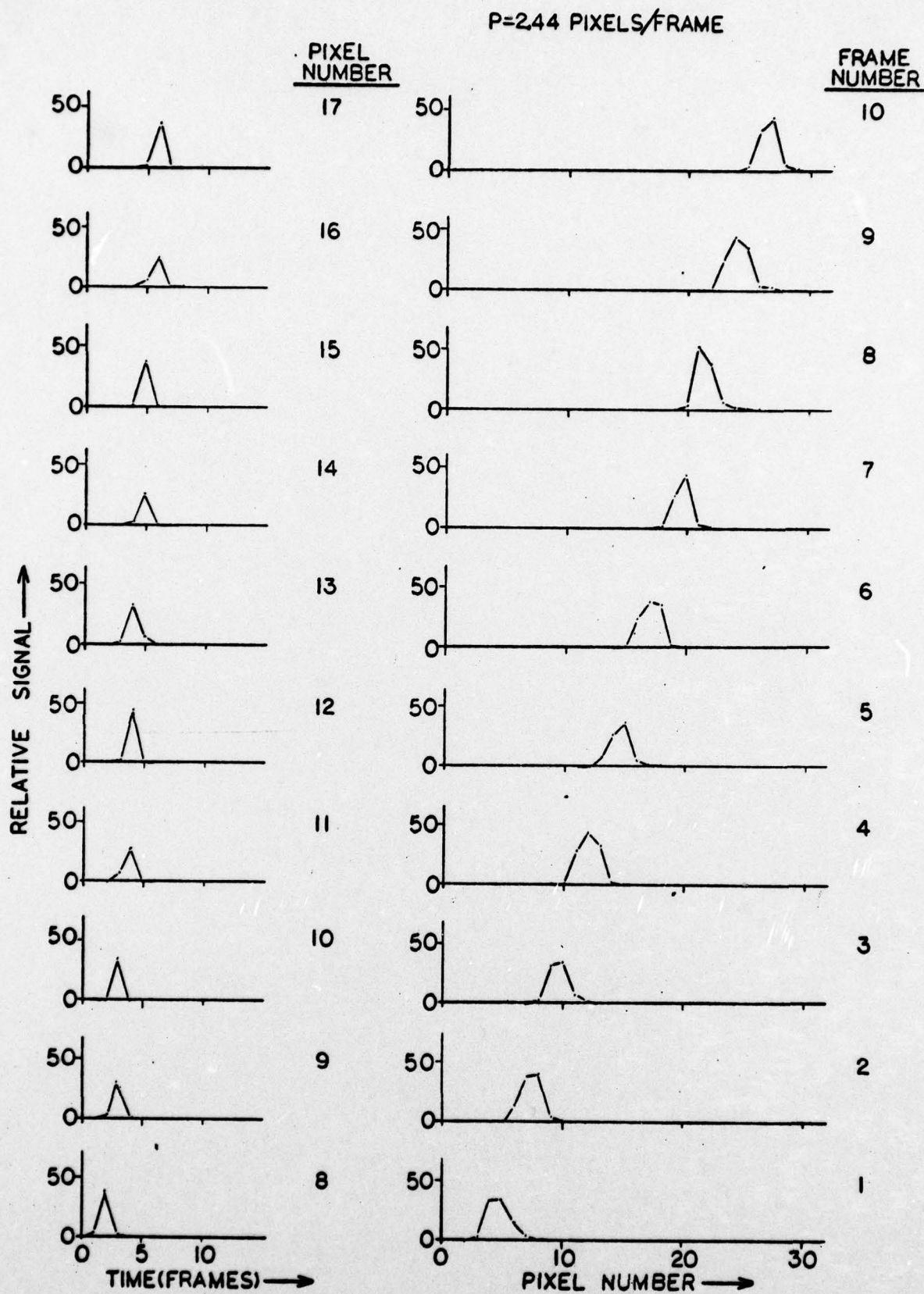


Figure 5.5. Scan Data at a Scan Speed of 2.44 Pixels/Frame

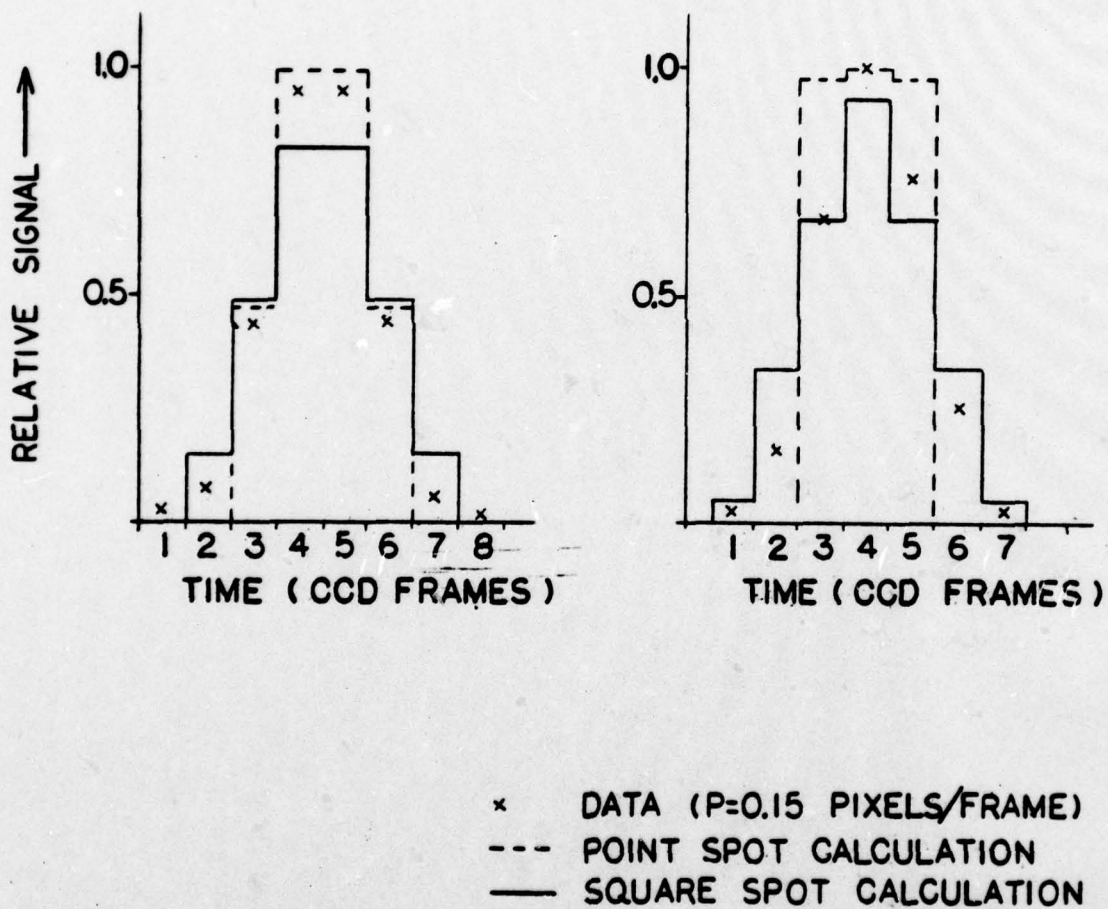


Figure 5.6. Signal Time Distribution at a Scan Speed of 0.15 Pixels per Frame

disappears showing the dead regions between pixels. At the highest speed, the spot appears in each pixel in only one frame and never disappears.

The right hand curves in Figure 5.2 through 5.5 show the corresponding spatial distributions along the row of pixels during several frames. The spatial distribution at low speed is sharply peaked (i.e., the spot appears in only one pixel at a time) and the signal varies dramatically from frame to frame. At high speeds, the spot is spread over several pixels in each frame and the peak signals are relatively constant.

The signal/time distribution at low scan speed provides information relating to the size of the light spot on the array. The measured signal/time distribution at a speed of 0.15 pixels per frame is compared to calculations in Figure 5.6. The calculations were performed for the CCD 202 geometry using both a point spot (dashed curves) and a square spot 18 μ m on a side with a uniform intensity distribution (solid curve). The two graphs show different phasing: the left one is for two equal signals at the peak, and the right one is for a single peak signal. The corresponding data were selected to approximate as closely as possible each phase. The comparison between the data and the calculations indicates an intensity distribution in between the two used for the calculations.

It was indicated in Section 4.0 of this report that the integrated signal in a single pixel as the spot passes over it should be inversely proportional to the scan speed (P) and the proportionality constant (for the CCD 202) should be 0.45

$n_0 \cdot I$, where n_0 is the instantaneous signal count rate in the entire spot and I is the CCD frame integration time (Equation 4.5). The product $n_0 \cdot I$ also gives the signal obtained with the spot stationary on one pixel. Figure 5.7 shows the reciprocal of the integrated signal as a function of the scan speed. The points marked "data" in Figure 5.7 (and succeeding figures) were obtained from the data shown earlier (as well as one data point at $P = 2.7$ not shown). The points marked "summed data" were obtained from the $P = 0.15$ data by summing consecutive frames and dividing by the number of frames summed. This analytical procedure yields data equivalent to that which would be obtained at a scan speed of 0.15 times the number of frames summed and was used to simulate data at $P = 0.31, 0.62, 1.24, 2.48,$ and 4.96 pixels per frame. The straight line in Figure 5.7 gives an excellent fit to the data and yields a value for $n_0 \cdot I$ of 214 (analog-to-digital converter units), in very good agreement with the peak signals observed at low scan speeds.

As explained in Section 4.0 of this report, target detection is based on the total signal produced as the spot crosses the array. To maximize the signal, the data from the CCD array must be shifted in phase with the spot motion on the array so that the maximum signal from the target is added from each frame. The maximum signals from the scan data are shown as a function of time (in CCD frame times) in Figure 5.8. The signals exhibit large peaks and valleys at low speeds and at high speeds the signal (peak) is lower but the signal remains relatively constant from frame to frame.

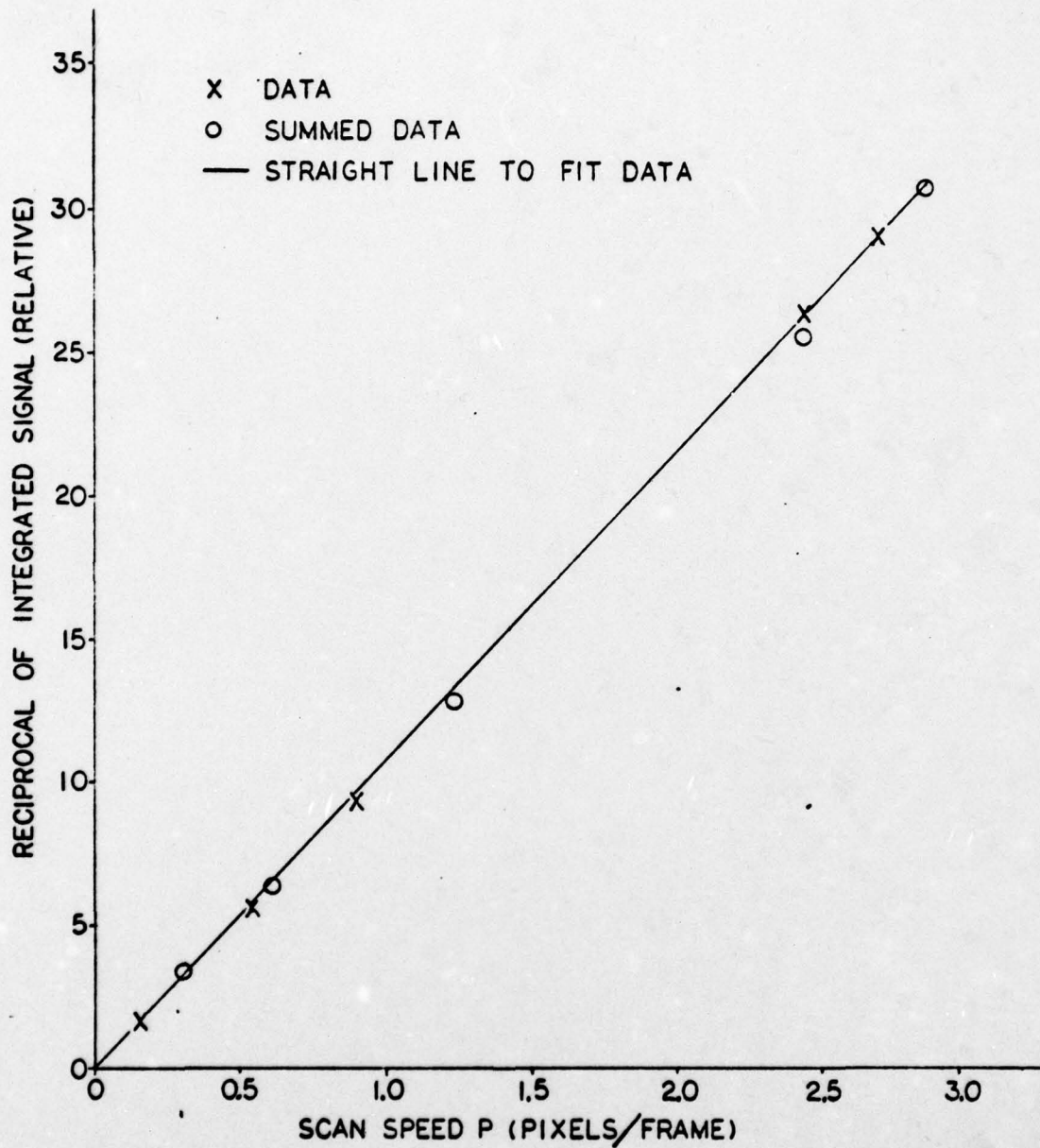


Figure 5.7. Reciprocal of Integrated Signals vs Scan Speed

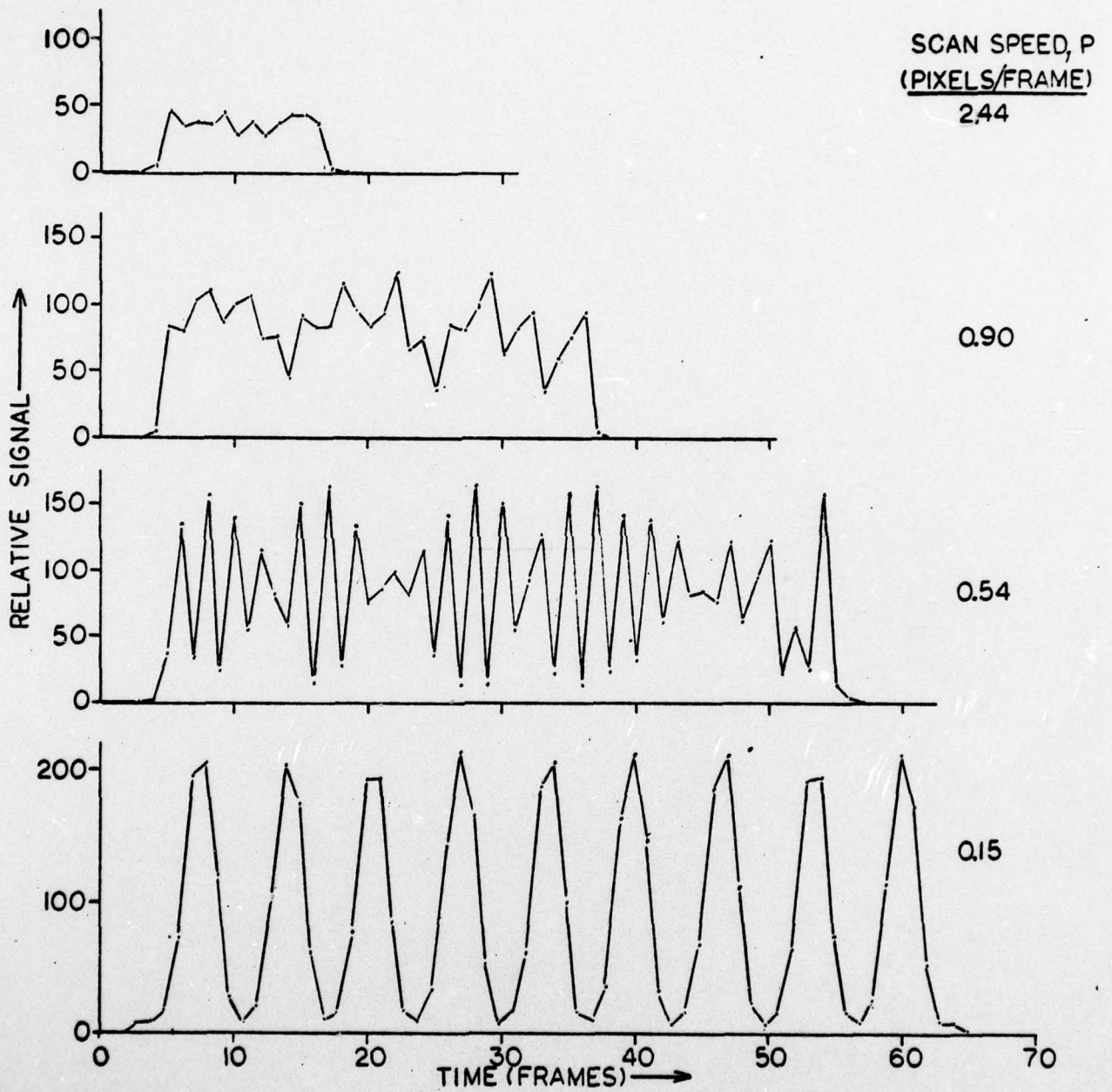


Figure 5.8. Maximum Signal from Each Frame vs Time for Various Scan Speeds

All of the data for this investigation were taken with the Fairchild CCD 202 array. However, since contiguous arrays are of interest for the TWS application, the output from such an array was simulated from the $P = 0.15$ data from the CCD 202. As shown in Figure 5.8, the data of $P = 0.15$ contains deep valleys corresponding to the times when the spot is between sensitive photosites. In a contiguous array, the peak signal would not fall below one half of the peak, and, therefore, data for a contiguous CCD array was approximated by selecting the CCD 202 signals that exceed one half of the peak. Due to the difference in geometry, the scan speed appropriate to the simulated contiguous data will be 2.22 times the scan speed of the corresponding CCD 202 data. Simulated contiguous CCD data was generated from the $P = 0.15$ CCD 202 data and higher scan speeds were obtained by the frame summing technique described above. In this way, contiguous CCD "data" were obtained for scan speeds of 0.34 (2.22×0.15), 0.68, 1.36, 2.72 and 5.44 pixels per frame.

The scan data were analyzed for both peak signals and average signals as the spot crossed the "array" of 30 pixels and the results are compared to calculations in the next two sections.

5.3 Peak Signal vs. Scan Rate

At slow scanning speeds the signal shows pronounced peaks and valleys as the spot crosses the array (see Figure 5.8). As explained in Section 4.0 of this report, the peak signals can be calculated in closed form for the spot geometries assumed

(point and square). Figure 5.9 presents a comparison of these calculations (summarized in Table 4.1) with the data. Three curves are shown for each CCD geometry: one for a point spot, one for a square spot with uniform intensity distribution, and the third curve is a simple arithmetic average of the first two. The curves were normalized at zero scan speed to the value of $n_0 \cdot I$ determined from the straight line fit to the integrated signal data (Figure 5.7). The data fall between the two calculations, perhaps favoring the point spot at very slow speeds. At higher speeds, above about $P = 0.9$ pixels per frame for the CCD 202 and about 1.8 pixels per frame for the contiguous CCD, the two calculations give the same result. The effect of spot size on the signal is greatest at about 0.45 pixels per frame for the CCD 202 where the square spot calculation is about 28% lower than that for the point spot. Similarly, the effect is greatest for the contiguous CCD at about 1 pixel per frame where the square spot result is about 25% lower than that for the point spot.

5.4 Average Signal vs. Scan Speed

In order to determine the total signal obtained using the shift-and-add integration (SAI) technique as a target crosses the array, the average signal per pixel per frame was determined by summing the maximum signal from each frame and dividing by the number of frames needed for the spot to cross the array. The results are presented in Figure 5.10 along with the calculations outlined in Section 4.0. Again, three curves are shown for each CCD geometry indicating the calculations for

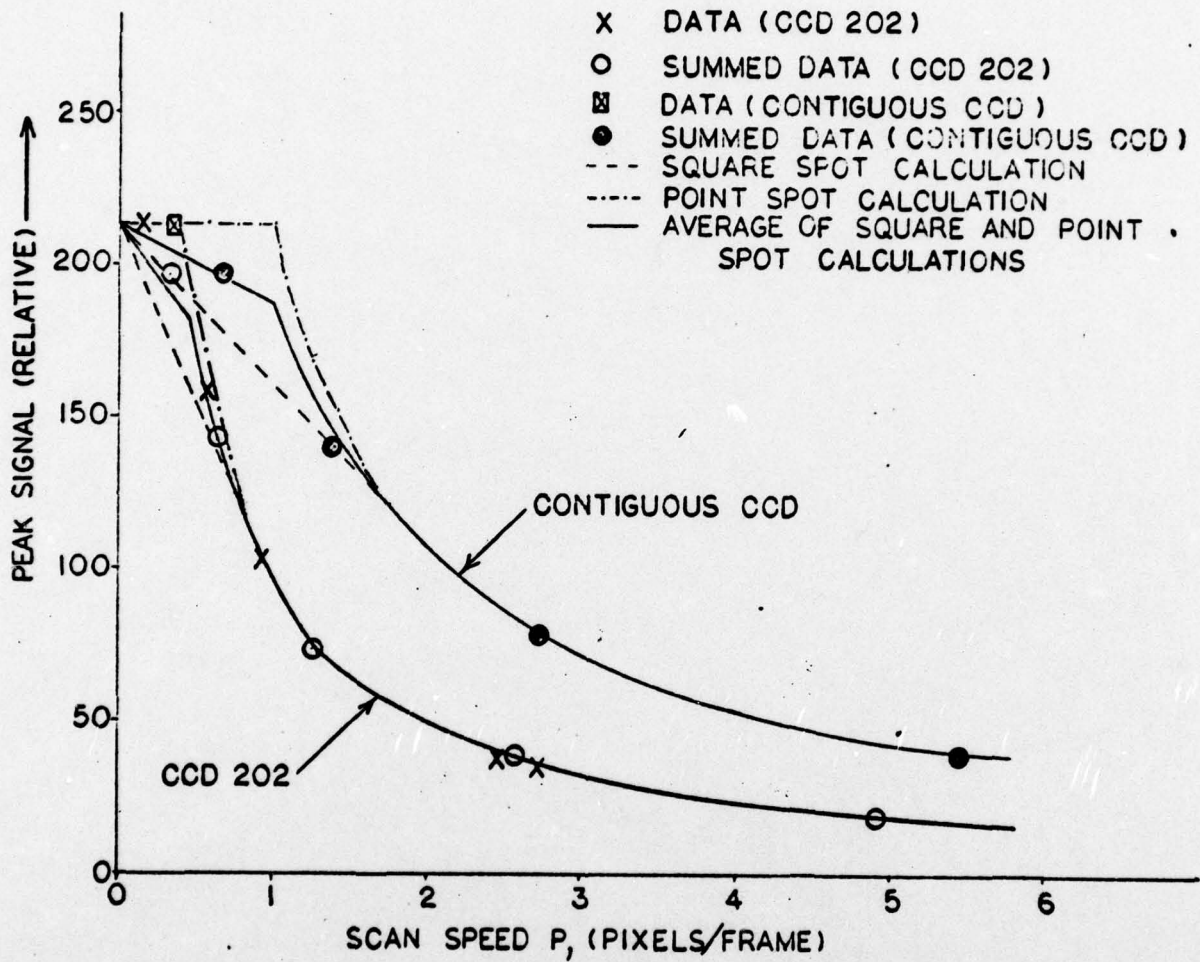


Figure 5.9. Peak Signals per pixel per frame vs Scan Speed for CCD 202 and Contiguous CCD. The data for the contiguous CCD were derived analytically from the CCD 202 data.

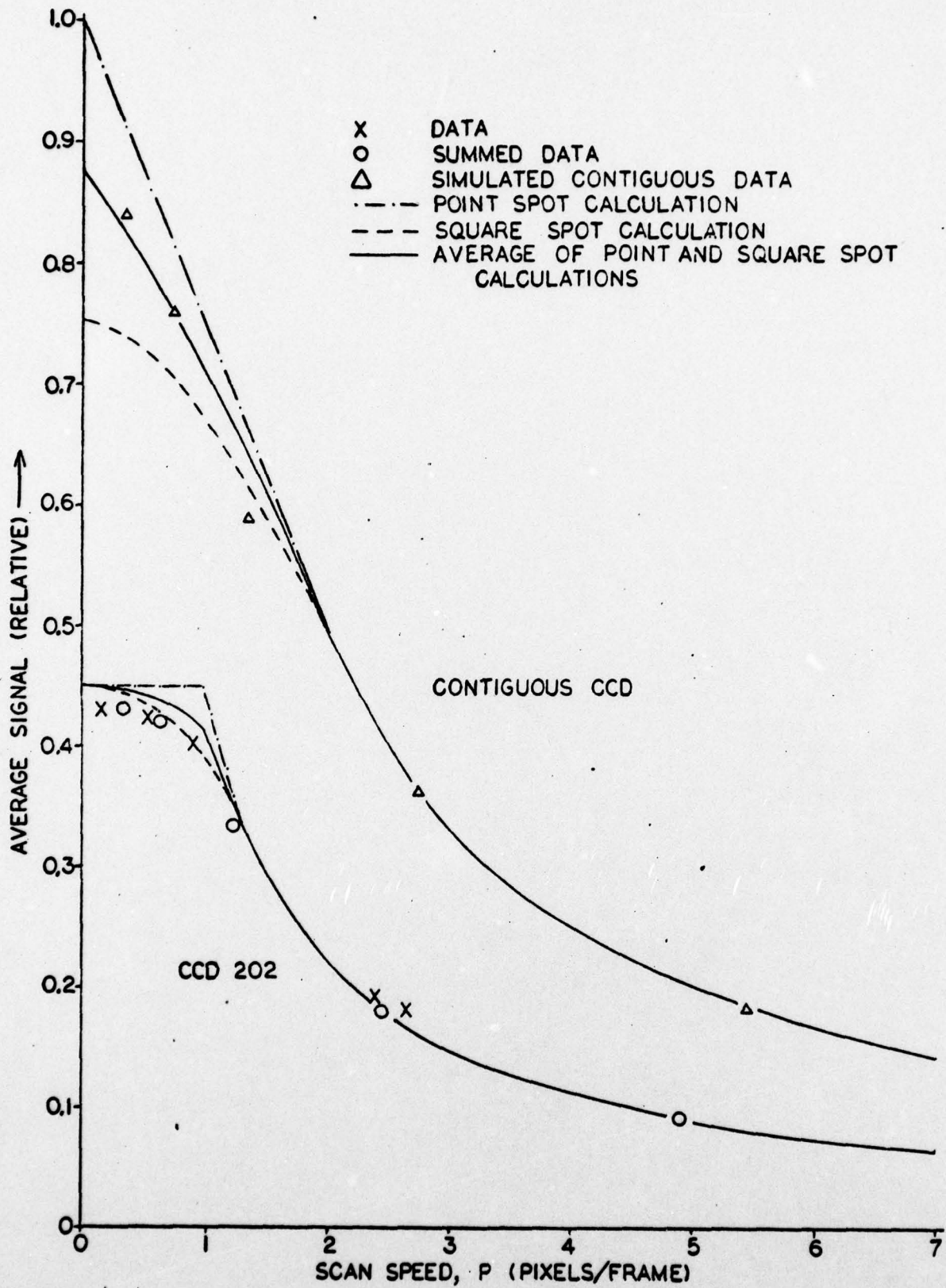


Figure 5.10. Relative Average Signal per pixel per frame vs Scan Speed for CCD 202 and Contiguous CCD

a point spot, a square spot and the average of the two calculations. The data and curves have been normalized to $n_0 \cdot I = 1$ at zero scan speed to indicate only the relative effect of sensor motion on the signal.

For the contiguous CCD, the data again fall between the two calculated limits. For the CCD 202, the data fall somewhat low at slow speeds. The reason for this slight systematic disagreement is not known but it is roughly the same size as the experimental uncertainties and is too small to have any significant effect on the results or conclusions of this study.

The curves for the average of the point spot and square spot calculations were used for the effect of sensor motion on the signal in the calculations of the sensor performance to be presented in Section 6.0.

5.5 Shift-and-Add Integration

In order to illustrate the shift-and-add integration (SAI) technique used to predict sensor performance, a simulation using actual scan data was performed and the results are shown in Figure 5.11. The data used were taken at a scan speed of 2.44 pixels per frame and the total shift (in the x-direction) used for each frame is shown as a solid curve (staircase) at the top of Figure 5.11. The dashed curve represents a shift of 2.44 pixels per frame, which in reality had to be approximated using integer shifts. The lower four curves show the resultant signals after 1, 2, 4, and 8 frame integrations. Although the spot width increases somewhat due to the use of integer shifts, the central two pixels accumulate signals in direct

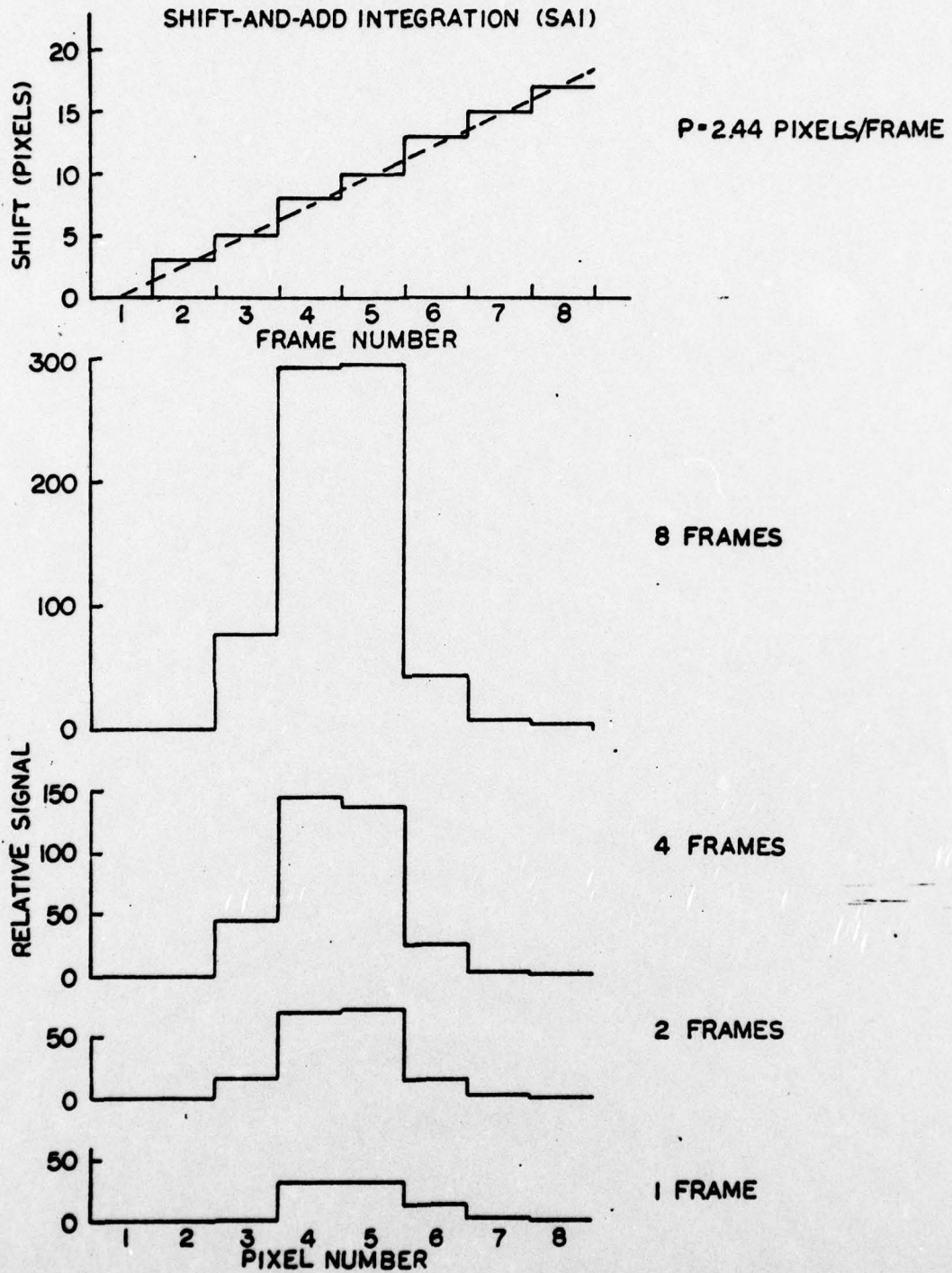


Figure 5.11. Shift-and-Add Integration Simulation

proportion to the number of frames summed. At slow scan speeds the situation would appear slightly different since each frame would not necessarily be shifted relative to the one immediately preceding it and the accumulation of signals would not be uniform. However, for a sufficiently large number of frames, the total integrated signal would still be equal to the average signal per frame multiplied by the number of frames.

5.6 Photoelectron Signal Distributions

In order to predict the Sensor performance, the variation in signal from one observation to the next must be determined so that the probability of obtaining a signal greater than a pre-determined threshold may be calculated. The present study assumes a constant light intensity from a target during the period of observation and, therefore, only noise sources associated with the detector and readout system will be considered.

In order to determine realistic signal variations, a Fairchild CCD 202 was irradiated with electrons in the electron damage test system. During irradiation with a constant average electron flux rate, the signals from a single pixel were repetitively measured and stored for successive frames and a histogram of frequency of occurrence vs relative signal was constructed. Examples of such histograms are presented in Figures 5.12, 5.13, and 5.14 for different electron flux rates at an electron energy of 18 kev. Since these distributions are approximately Gaussian in shape (see dashed curves), standard deviations, σ , were

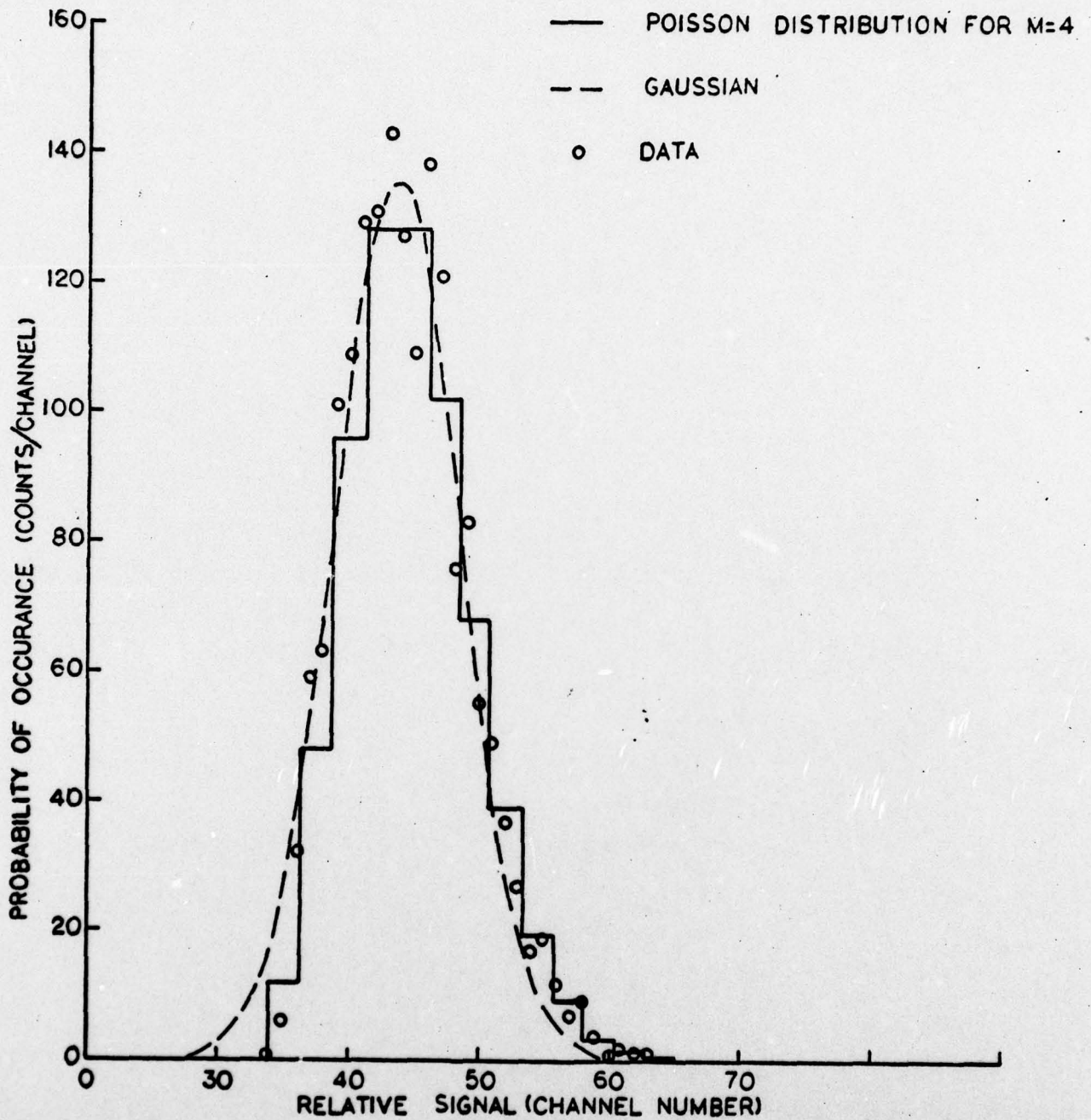


Figure 5.12. Signal Distribution for 18 keV Electrons in One Pixel of CCD 202 at a Mean Flux Rate of About 4 Electrons per pixel per Frame. Zero Signal Corresponds to Channel 33.

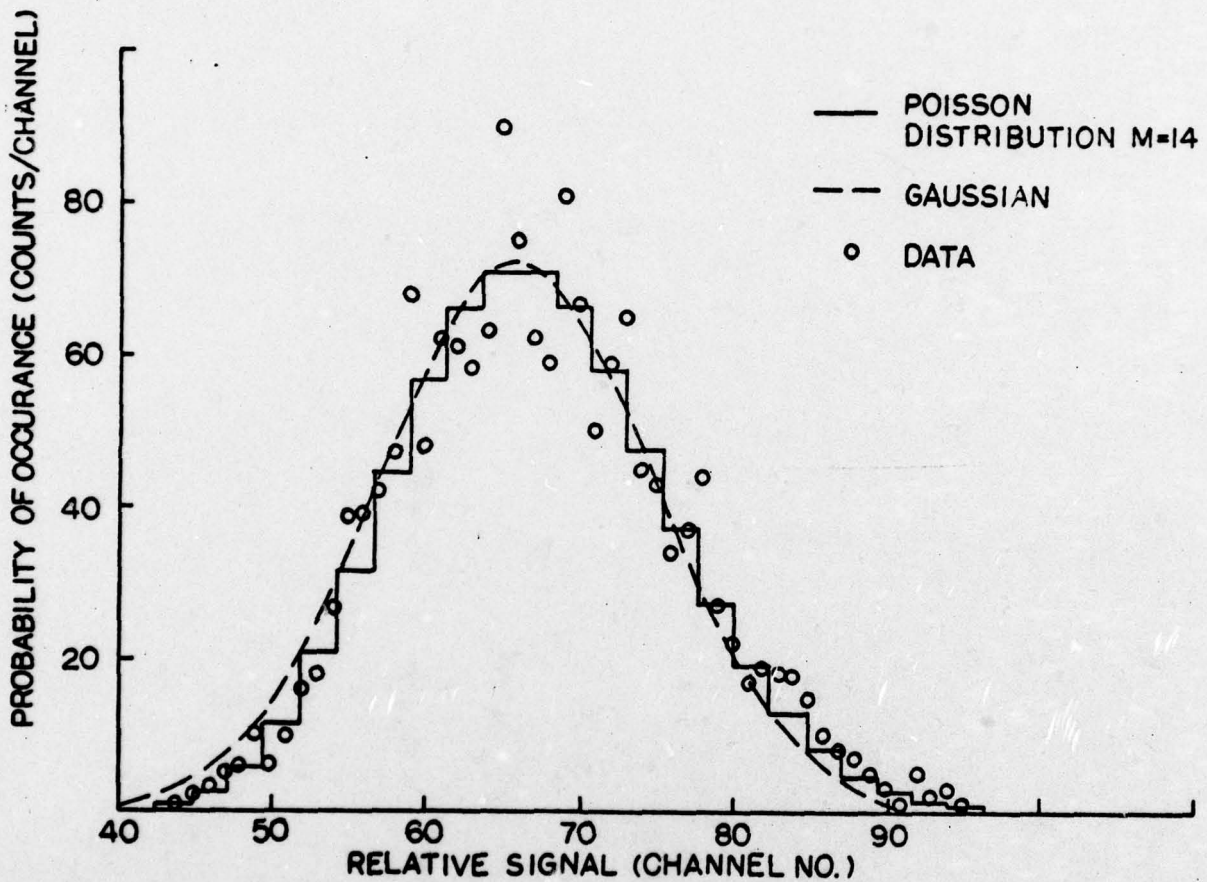


Figure 5.13. Signal Distribution for 18 keV Electrons in One Pixel of a CCD 202 at a Mean Flux Rate of About 14 Electrons per Pixel per Frame. Zero Signal Corresponds to Channel 33.

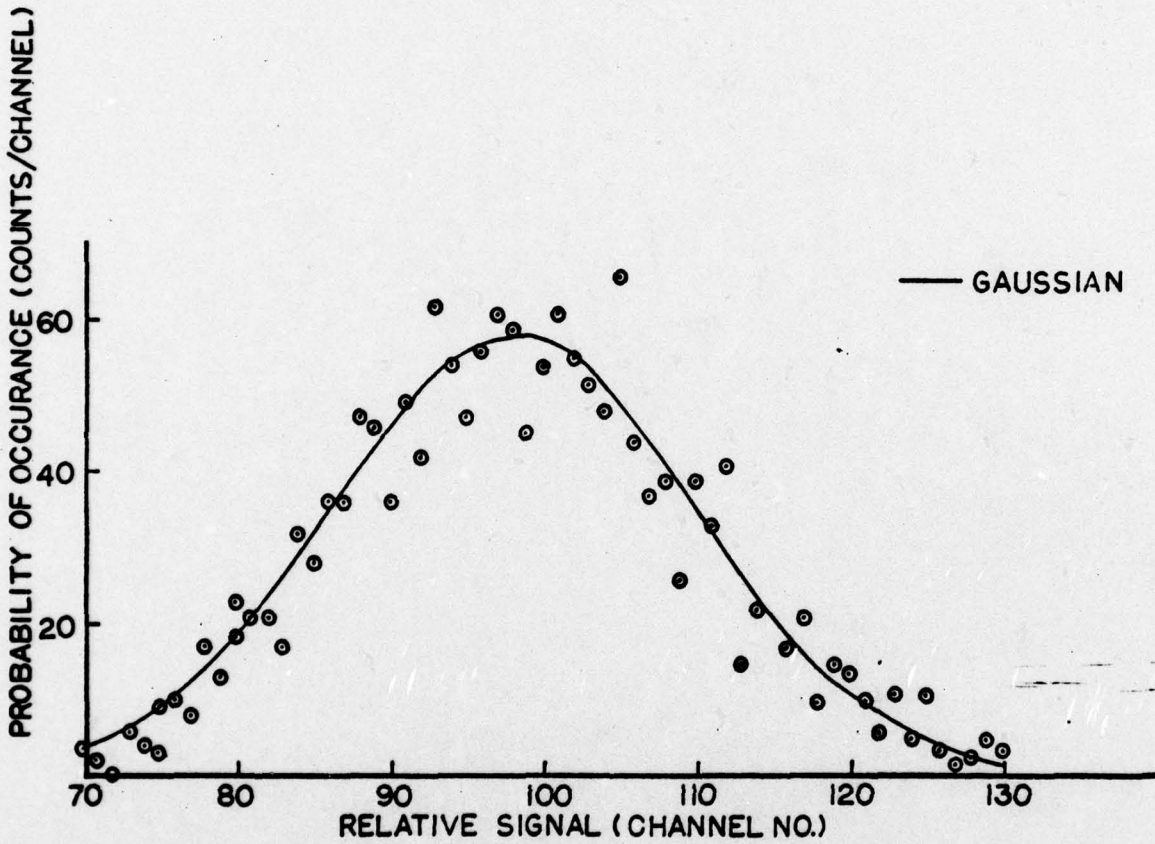


Figure 5.14. Signal Distribution for 18 keV Electrons in One Pixel of a CCD 202 at a Mean Flux Rate of About 25 Electrons per Pixel per Frame. Zero Signal Corresponds to Channel 33.

calculated for each set of data by dividing the full width at half maximum (FWHM) by 2.35:

$$\sigma = \frac{(\text{FWHM})}{2.35} \quad (5.1)$$

Assuming that the total width is due to the statistical distribution in the number of electrons combined with electronic readout noise we get:

$$\sigma^2 = \sigma_o^2 + \sigma_s^2 \quad (5.2)$$

where σ_o and σ_s are the standard deviations due to electronic noise and electron statistics respectively. For a normal (Gaussian) distribution,

$$\sigma_s^2 = N_e \quad (5.3)$$

where N_e is the mean number of electrons in the distribution. Combining Equations 5.2 and 5.3 we obtain:

$$\sigma^2 = \sigma_o^2 + N_e \quad (5.4)$$

The observed signal, S_e , is the mean of the distribution and is proportional to the mean number of electrons detected:

$$S_e = kN_e \quad (5.5)$$

The proportionality constant depends on the electron gain in the CCD as well as the net gain of the electronics from the CCD readout shift register through the analog-to-digital converter (ADC). Combining Equations 5.4 and 5.5 we obtain:

$$\sigma^2 = \sigma_0^2 + S_e/k \quad (5.6)$$

Therefore, if σ^2 for each distribution is plotted as a function of the observed mean signal (S_e), the results should fall along a straight line with slope $1/k$ and y-axis intercept ($S_e = 0$) of σ_0^2 . Figure 5.15 shows such a plot for the present data. The fit to a straight line is excellent with a slope of 2.37 ADC channel numbers per electron and a σ_0 of about 0.3 electrons. This small detector-associated noise contribution is negligible for signals above a few electrons per frame. Since virtually all of the signals encountered in this operation are larger than this, the detector-associated noise was neglected, and only fluctuations due to photoelectron statistics were considered.

Using the above calibration (2.37 channel numbers per electron), the mean numbers of electrons for the distribution were calculated by dividing the shift of the peak in ADC units by 2.37. The results for the distributions shown in Figures 5.12, 5.13, and 5.14 were approximately 4, 14, and 25 electrons per pixel per frame respectively.

The Poisson distributions for mean values of 4 and 14 were calculated and are compared to the data in Figures 5.12 and 5.13, along with the Gaussian distributions with the appropriate widths and heights to fit the data. In both cases, the two calculations seem to give about equally good representations of the data over the central part of each distribution while the Poisson distributions give better fits at the edges. The Gaussian distributions overestimate the data at the left

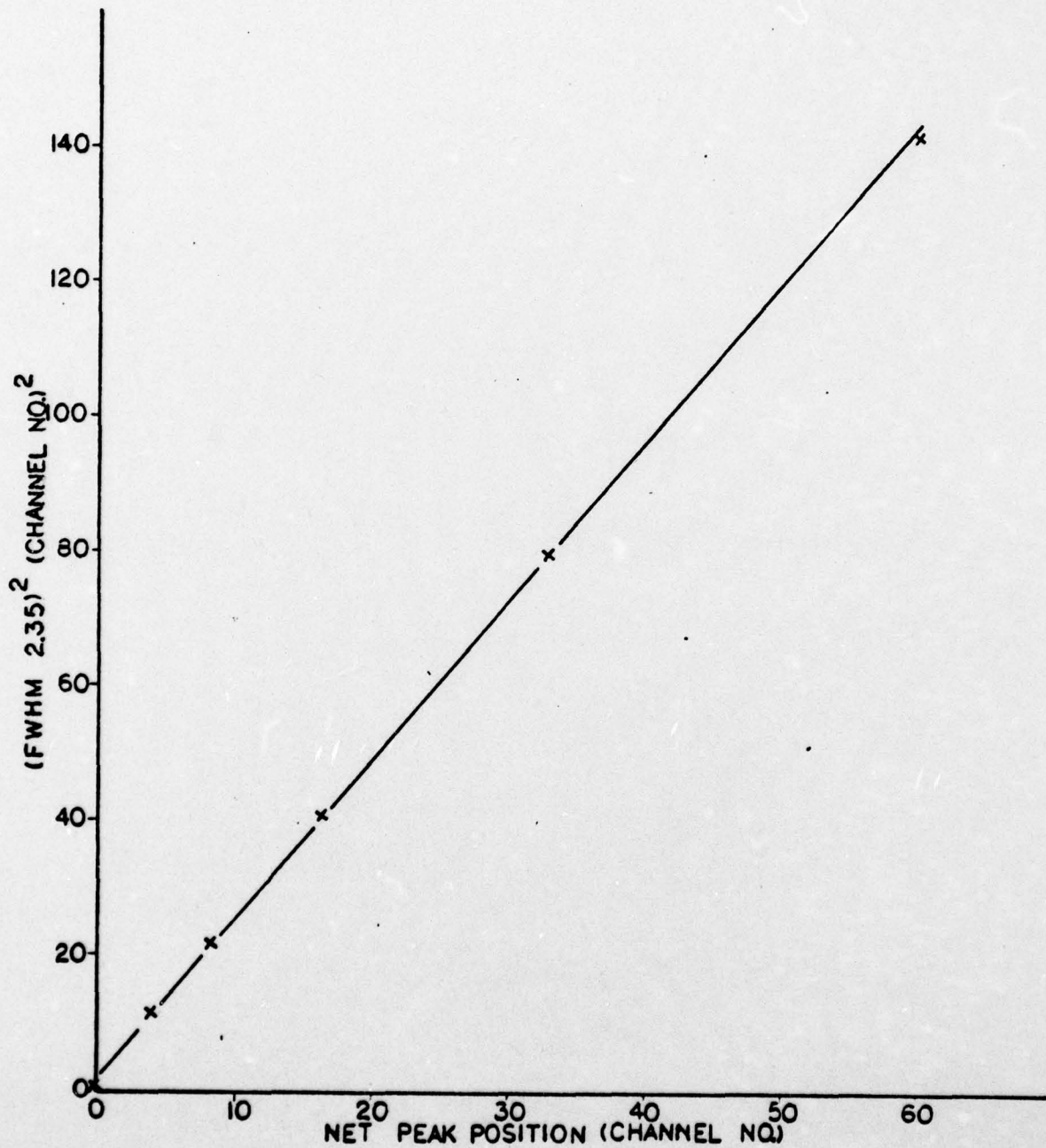


Figure 5.15. σ^2 vs Net Peak Position for Electron Signal Distributions

(low signal) edge and underestimate the data at the right edge.

In Figure 5.14, only the Gaussian calculation is presented and the fit to the data is quite good. However, the tendency to overestimate the left edge of the peak and underestimate the right edge is apparent here, also. The quantity of interest in determining the threshold, detection probability (DP) and background event probability (BEP) is the fraction of signals that exceed a given threshold. Figure 5.16 shows the fraction of signals which exceed the threshold as a function of the threshold for various distributions. The threshold is expressed in standard deviations from the mean for a Gaussian distribution and \sqrt{N} for a Poisson distribution with a mean of 14 ($\sqrt{14} = 3.74$). The data points were derived from the distribution shown in Figure 5.13 and the standard deviation for the data was calculated using Equation 5.1 (i.e., $\text{FWHM}/2.35$).

The Gaussian distribution represents the data very well for fractions above 90%, demonstrating the validity of using the Gaussian distribution to obtain the threshold given a required detection probability (see Section 4.0). On the large signal edge of the distribution, the Gaussian distribution falls below the data which agrees more closely with the Poisson distribution, demonstrating the rationale behind the use of the latter for BEP determination.

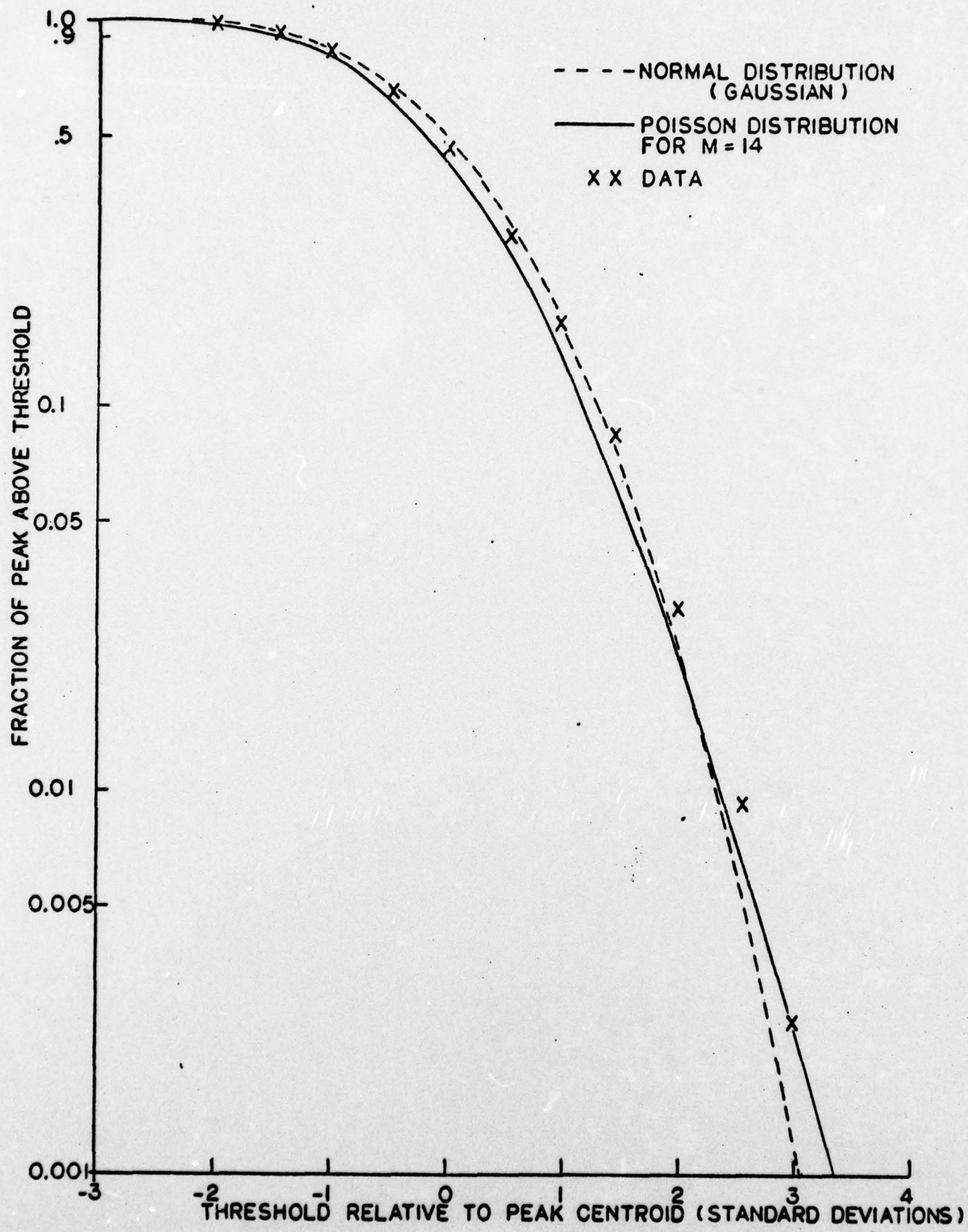


Figure 5.16. Fraction of Distribution Exceeding Threshold vs Threshold in Standard Deviations (\sqrt{N}) from the Mean Value (N)

6.0 SENSITIVITY CALCULATIONS

Using the signal and background intensities presented in Section 3.0 and the analytical techniques described in Section 4.0, calculations of the ICCD sensor performance under various operating conditions were performed. The sensor performance was described in terms of the Background Event Rate (BER) which is the rate at which CCD pixels, irradiated only by the background, produce signals which exceed the threshold necessary to achieve a specified detection probability (DP). It was shown in Section 5.0 that the CCD readout noise was negligible compared to fluctuations due to photoelectron statistics for the signals of interest to this study. Therefore, the present analysis was based on the assumption that variations in the observed signals for specific target and background intensities were due entirely to photoelectron statistics. In addition, as illustrated in Section 5.6, for the purpose of calculating the threshold level, the signal distribution was assumed to be normal (Gaussian) in shape. In order to provide a conservative estimate of sensor performance, the BER was calculated using a Poisson distribution.

The parameters for the optics used in the analysis were taken to be 73mm focal length and 4.62 sq. cm for the net area of the aperture. Two CCD geometries were used. The first was that of the CCD 202 (18 μ m x 30 μ m photosites separated by 22 μ m dead spaces) and the second was similar except no dead spaces were used (i.e., contiguous geometry). The number of pixels in the X (or scan) direction was varied from 10 to 100 while

in the Y direction the number was fixed at 100. The efficiency factor, which expresses the fraction of the spot which crosses a given pixel, was conservatively assumed to be 0.5. The area of sky covered was fixed at 13 degrees (X-direction) by nine degrees and the DP was generally assumed to be 0.99 although calculations for values as high as 0.999 were performed.

Observation times from 10 to 45 seconds were considered, and CCD frame integration times between 2 and 50 msec were used. As explained in Section 3.0, the intensity of the target was assumed to be between 6 and 10 visual magnitudes while the background was varied between -3 and 2 visual magnitudes per square degree corresponding to solar elongation angles (see Section 3.0) from less than approximately 10 degrees to 33 degrees.

Figure 6.1 presents the calculated BER as a function of observation time for various background count rates between 100 ($M_b = 2$) and 10,000 ($M_b = -3$) counts per pixel per second. The array geometry was that of the CCD 202 with 100 x 100 pixels and a frame integration time of 0.05 sec. The DP was taken as 0.99 for a target intensity of $M_v = 6$. The results indicate that the BER for a given background intensity is a very strong function of observation time. For all of the backgrounds used, a reasonable (i.e., less than 1 minute) observation time can be found which yields a BER of less than 10^{-6} per second (1 event per 11.6 days). This observation time is shown in Figure 6.2 as a function of the background count rate. Over the range considered here, the observation time is not a very strong function

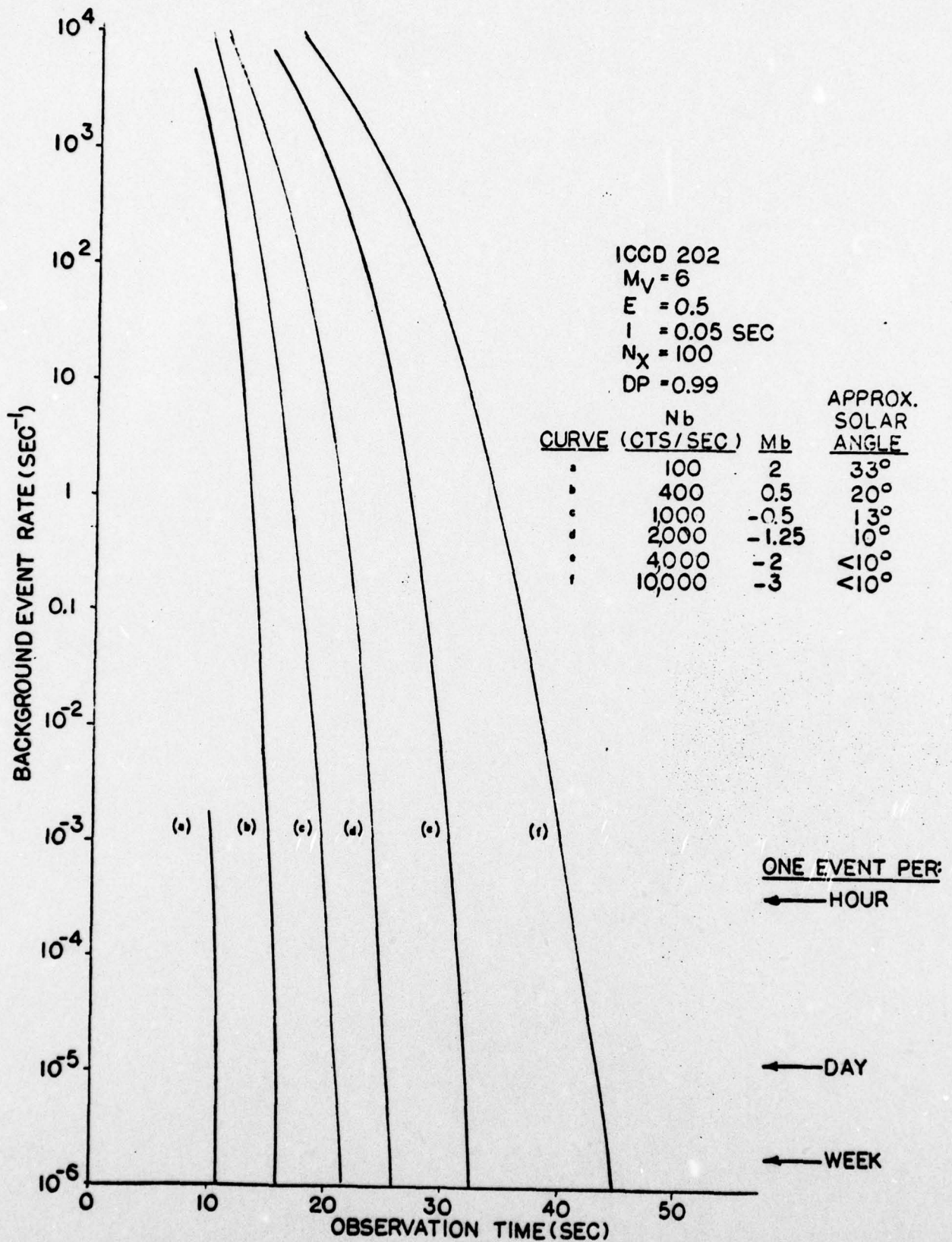


Figure 6.1. Background Event Rate vs Observation Time for Various Background Intensities and $M_V = 6$ Target

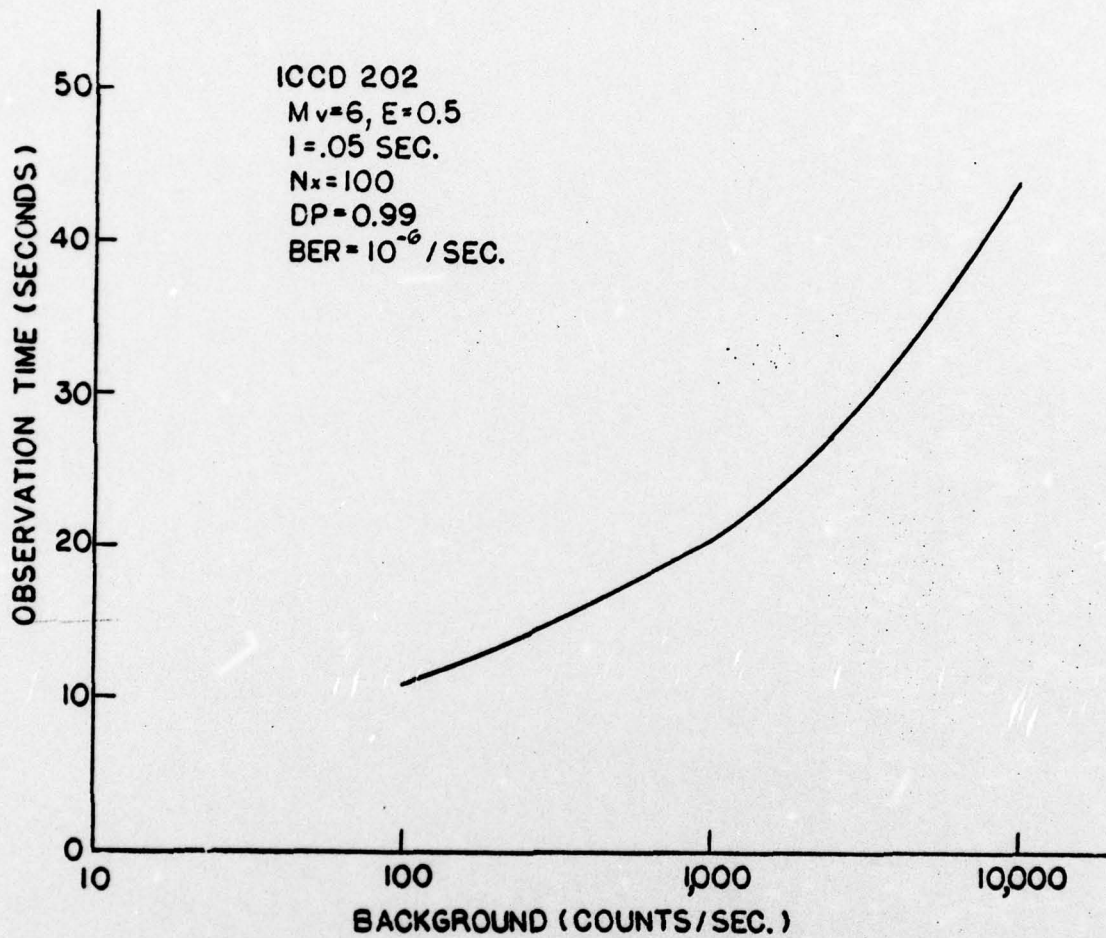


Figure 6.2. Observation Time Required to Produce a Background Event Rate of 10^{-6} per Second vs Background Count Rate for $M_v = 6$ Target

of background rate, merely doubling for an order of magnitude increase in background.

The performance can be improved considerably by reducing the CCD frame integration time as shown in Figure 6.3. For these calculations, the observation time was fixed at 30 sec and both CCD 202 (solid curves) and the contiguous geometries (dashed curves) were used, both with 100 x 100 pixels. The target intensity used here had a visual magnitude of $M_V = 7$.

For each specific background intensity, the BER drops sharply as the CCD frame time is reduced. This reduction is due to the relative increase in signal as the scan speed (P) across the array decreases (see Figure 5.10). The leveling off of the average signal vs scan speed (Figure 5.10) for the CCD 202 causes the BER (Figure 6.3) to level off at short frame times. The scale at the top of Figure 6.3 shows the scan speed (P) in pixels per frame for the two array geometries. Over most of the frame time range of Figure 6.3, the CCD 202 is somewhat better than the contiguous CCD for the same CCD frame time. For very short frame times (less than about 10 msec) the contiguous CCD is superior to the CCD 202 because its average signal continues to increase at low scan speeds, P (Figure 5.10).

The conclusion from Figure 6.3 would appear to be to use a contiguous array with as short a frame time as possible. However, other effects, not taken into account in the present analysis, may affect this conclusion. One effect is that at very short frame times the average number of photoelectrons per frame becomes small, and the electronic readout noise (neglected here)

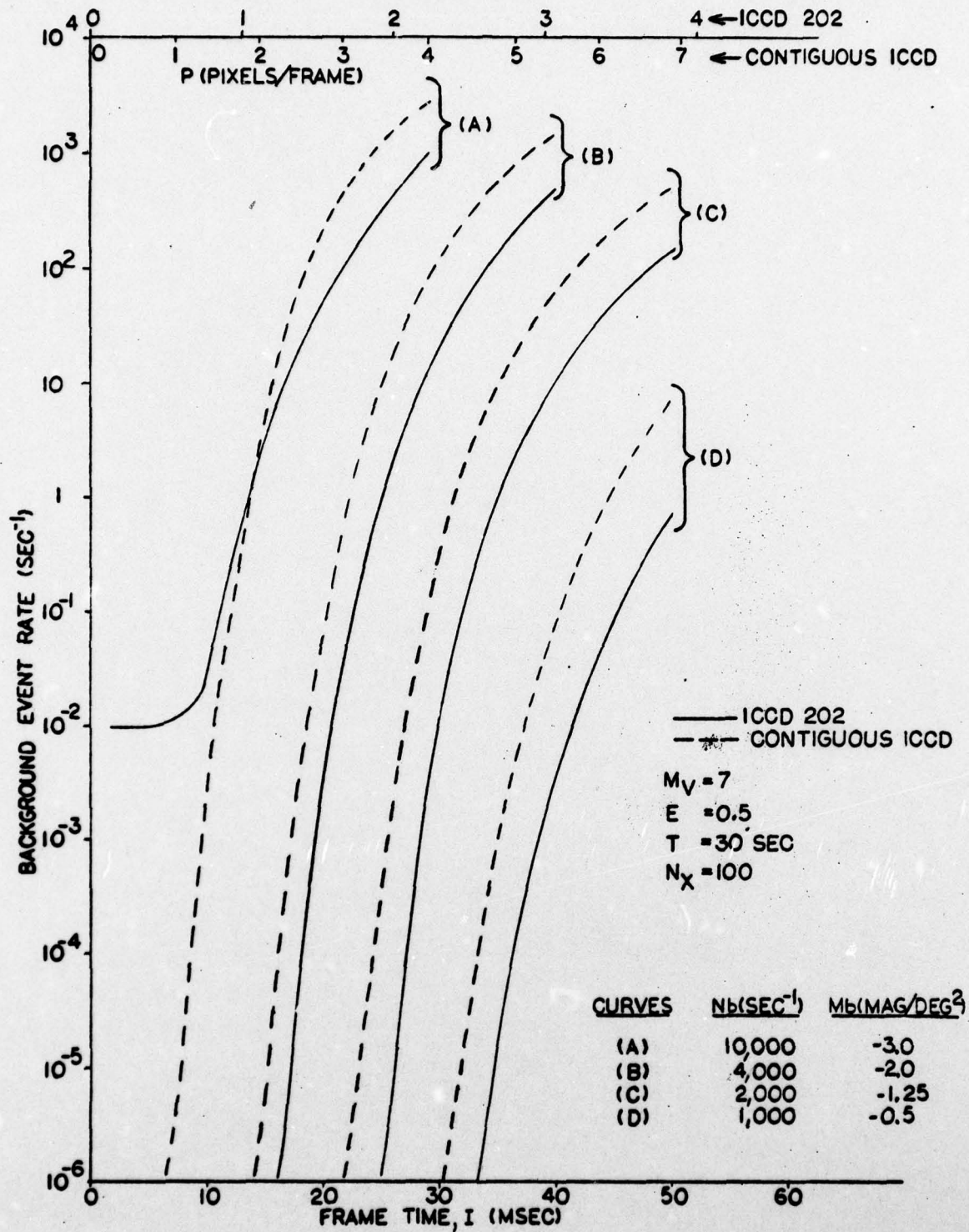


Figure 6.3. Background Event Rate vs CCD Frame Integration Time for Various Background Intensities

may become important, especially in low background regions where increased sensitivity is desirable. Another effect that becomes important at short frame times is that the CCD pixel readout rate may become excessively high, as illustrated in Figure 6.4. High pixel readout rates are undesirable due to the increase in the bulk, weight and power requirements of signal processing and memory electronics as the required operations speed increases.

It seems desirable to limit the pixel readout rate to less than 1 MHz, perhaps to 0.6 MHz. Referring to Figure 6.4, this limits the frame time for a 100 x 100 array to about 20 msec. However, as shown in Figure 6.4, the pixel readout rate may be kept below 1 MHz for short frame times by reducing the number of columns (N_x) in the CCD array. This has the added benefit, shown in the upper curve in Figure 6.4, of reducing the size of the buffer memory required for fixed pattern subtraction and shift-and-add integration, each of which require a buffer memory at least as large as the array.

Figure 6.5 shows the effect on the BER of reducing the number of columns (N_x) in the array, which otherwise has the CCD 202 geometry. The increase in BER as N_x decreases appears to be less (at least for the higher backgrounds) than the decrease in BER with a decrease in frame time (I). This behavior strongly suggests that sensor performance equivalent to $N_x = 100$ at $I = 20$ msec can be maintained or exceeded with a CCD 202 geometry array with N_x of 50 operating at 10 msec frame time. For a contiguous array geometry, the number of columns may be

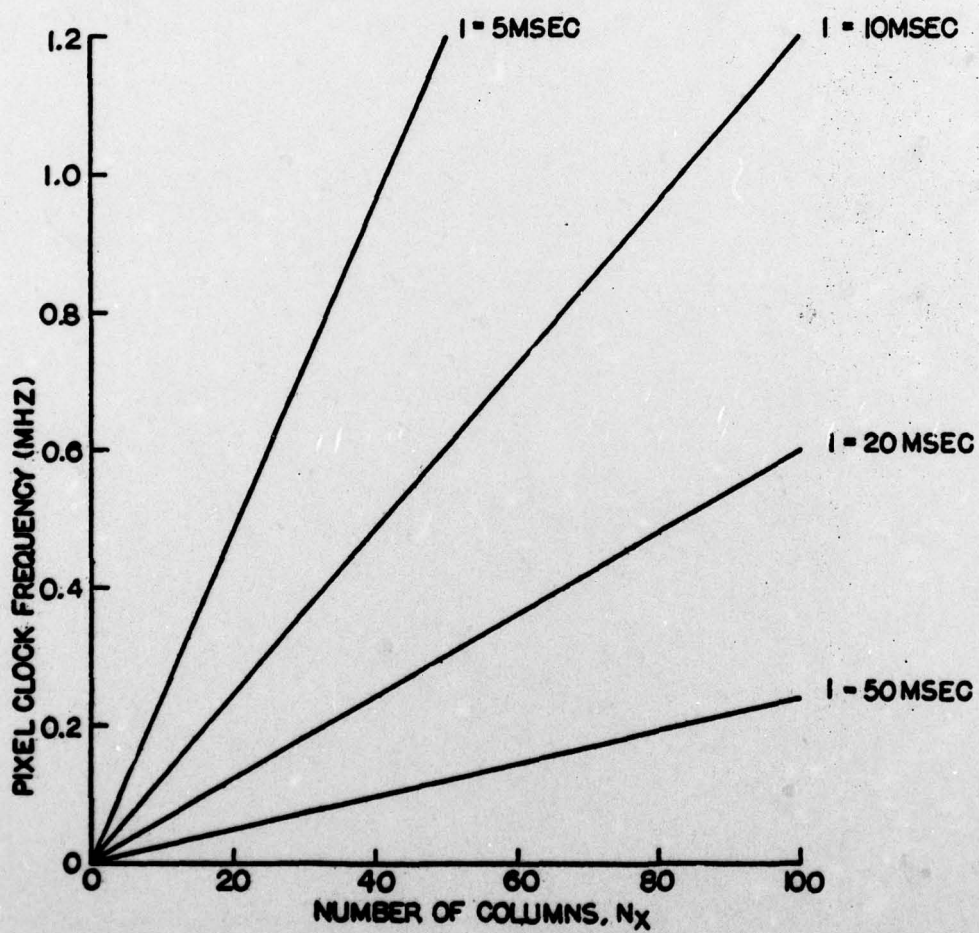
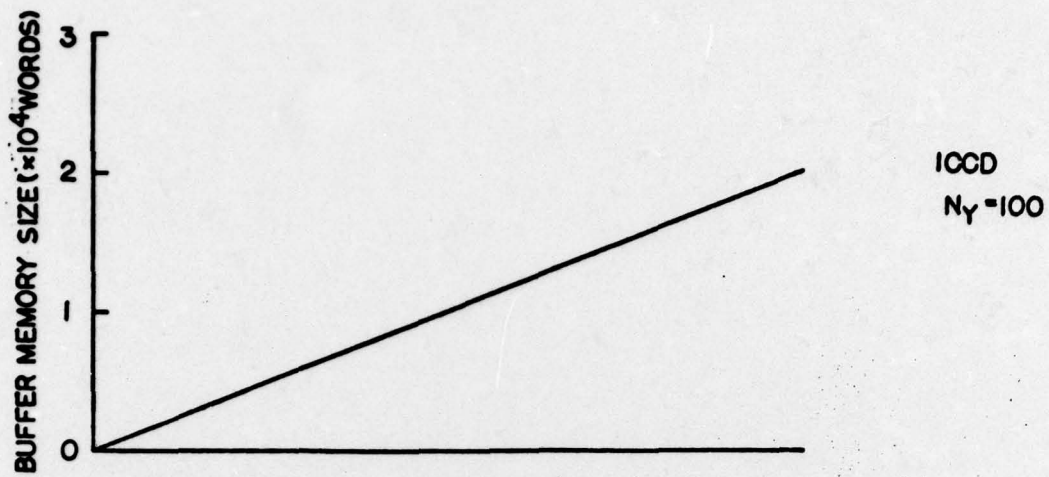


Figure 6.4. CCD Pixel Readout Frequency and Buffer Memory Size vs. Number of CCD Columns (N_x)

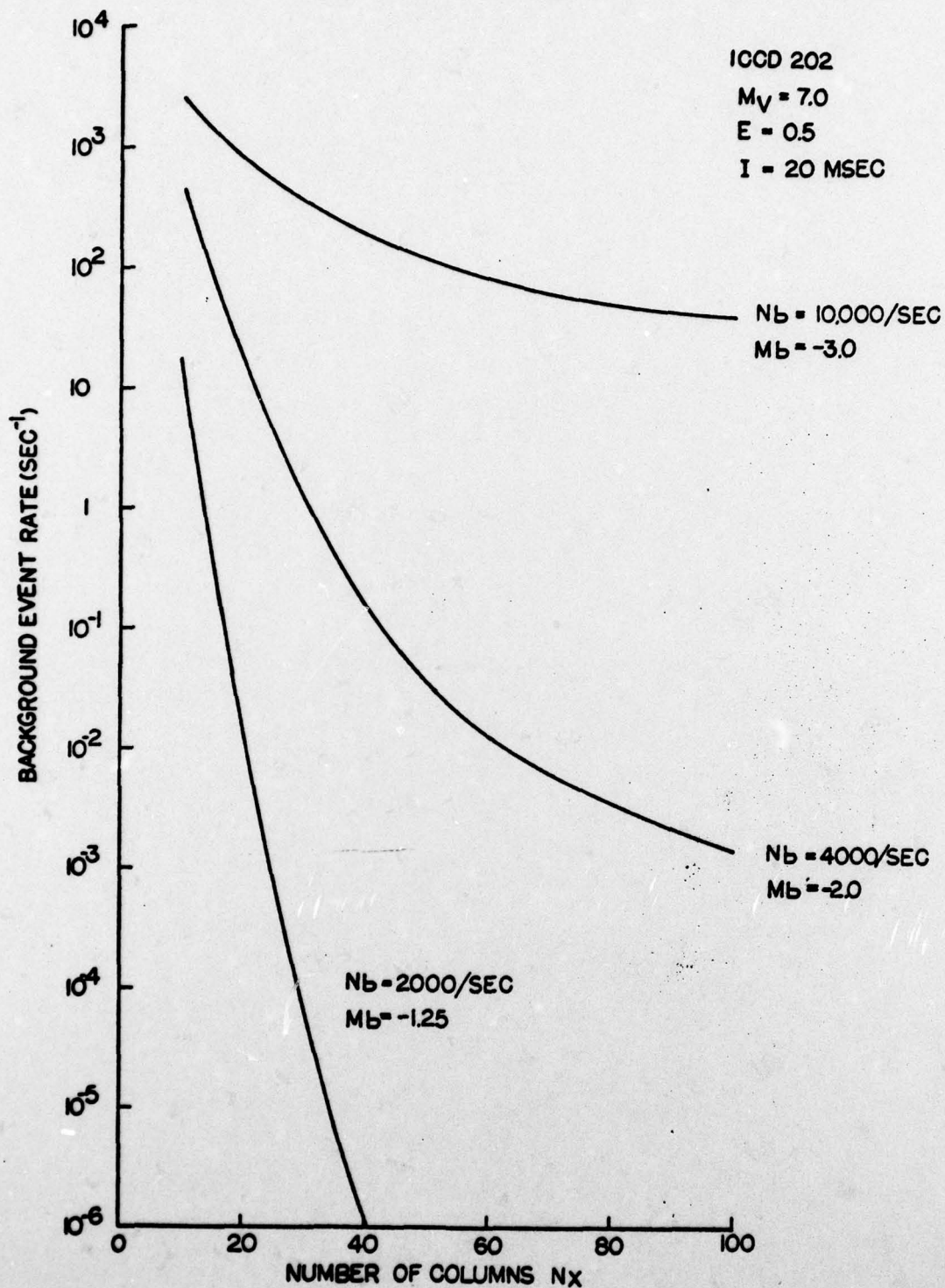


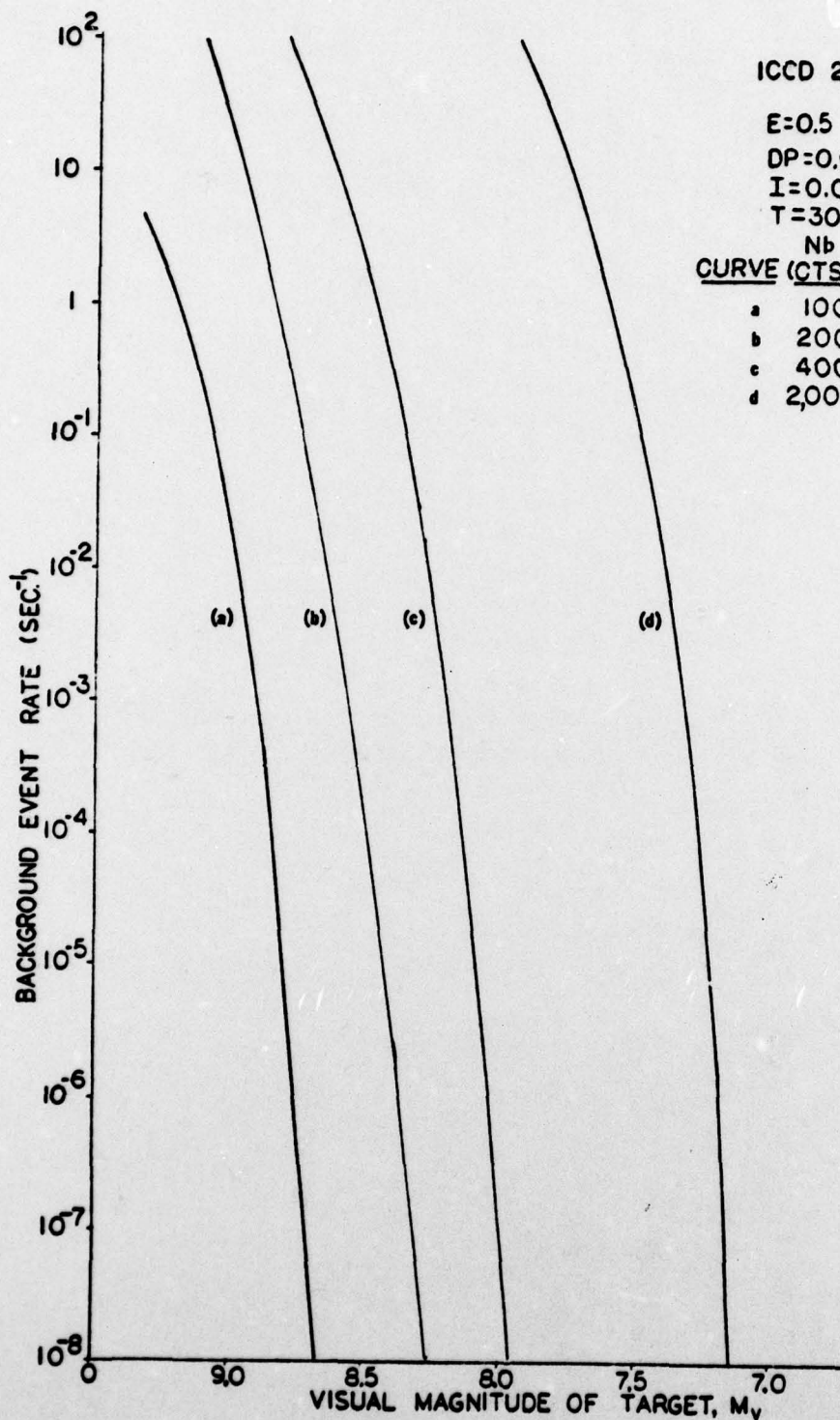
Figure 6.5. Background Event Rate vs Number of Columns in the Array for Various Background Intensities

reduced even further, perhaps even to 20 columns operating at $I = 4$ msec.

Figure 6.6 shows the BER for a CCD 202 geometry (100 x 100) array operating at a frame time of 20 msec. for various target and background intensities. For each background intensity, there is a limiting target intensity (LTI) below which the BER increases very rapidly. In order to quantify the present results, the LTI was defined as the target intensity which was detectable with a DP of 0.99 and a BER of 10^{-6} per second.

For all of the results presented so far, the signal was derated by a factor of two ($E = 0.5$) to allow for vertical misalignment between the spot and the rows of pixels. This value of E is actually the minimum expected and was used to provide a conservative estimate of the sensor sensitivity. For perfect alignment between the spot and the pixels, E has its maximum value 1.0. All values of E between 0.5 and 1.0 are equally likely, and so a more realistic estimate of the average value of E is 0.75. The increase in E from 0.5 to 0.75 (i.e., 50% increase in signal) is equivalent to a gain in sensitivity of 0.44 stellar magnitudes. The remaining results were calculated using $E = 0.75$.

The LTI for the CCD 202 geometry (100 x 100 pixels) array operating at a frame time of 20 msec is shown as a function of background intensity (in photoelectrons per pixel per second) is shown in Figure 6.7. These calculations were performed, using $E = 0.75$, for observation times of 30 and 60 sec. and detection probabilities of 0.99 and 0.999. Below a background



ICCD 202

E=0.5

DP=0.99

I=0.02 SEC.

T=30 SEC.

CURVE	N_b (CTS/SEC)	M_b	APPROX. SOLAR ANGLE
a	100	2	33°
b	200	1.2	25°
c	400	0.5	20°
d	2,000	-1.25	10°

Figure 6.6. Background Event Rate vs Target Intensity for Various Background Intensities

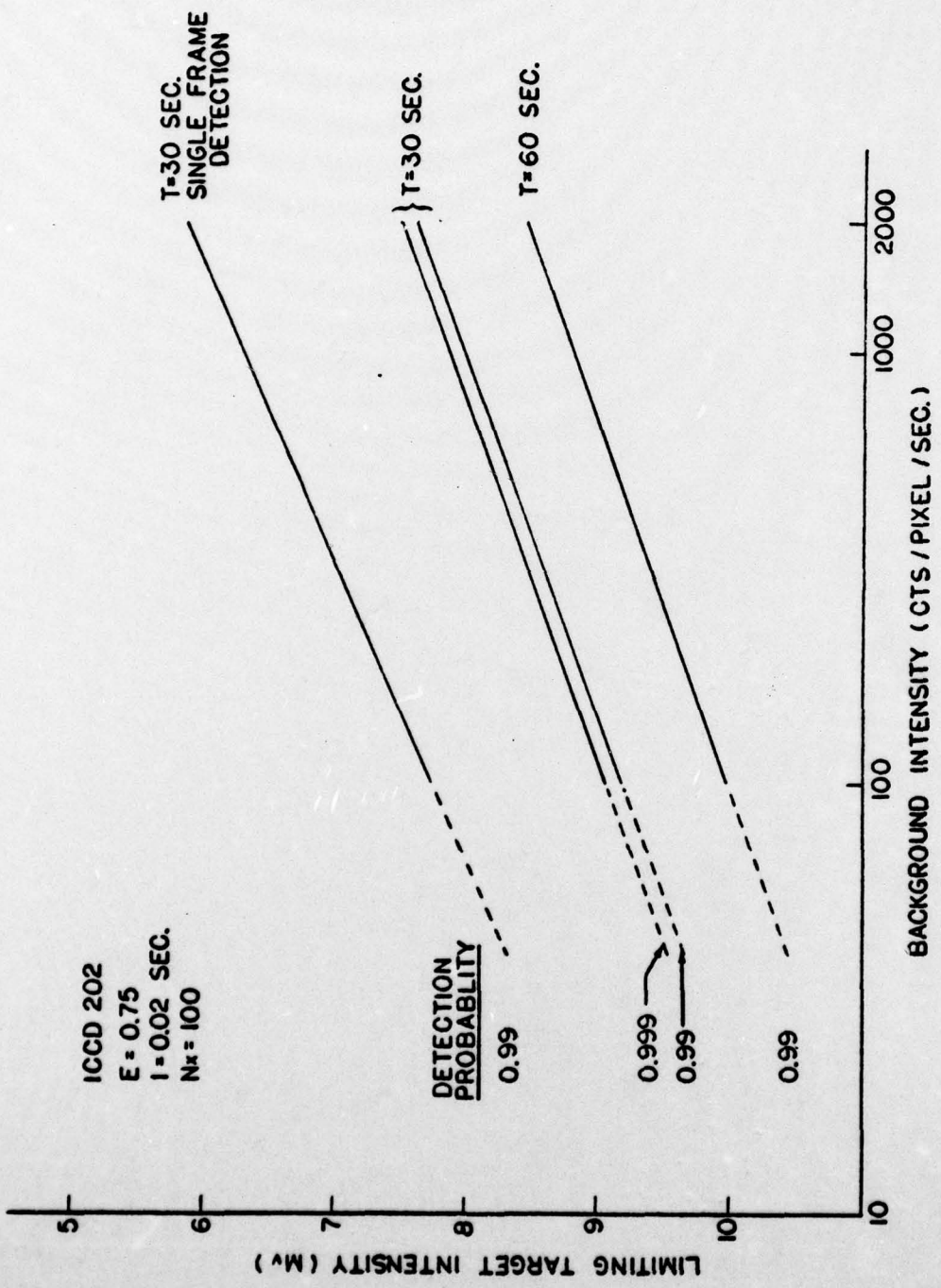


Figure 6.7. Limiting Target Intensity vs Background Intensity for Observation Times of 30 Sec. and 60 Sec.

intensity of 100 counts per pixel per second, the curves are dashed to indicate that the results may be inaccurate due to the small numbers of photoelectrons per frame detected and the fact that the analysis neglected the electronic readout noise.

The bottom curve ($T = 60$ sec) in Figure 6.7 shows the increase in sensitivity gained by doubling the 30 sec observation time used for the other curves. At a constant DP of 0.99, the resultant increase in sensitivity is approximately 0.8 stellar magnitudes over the range of backgrounds considered.

The curve marked "DP = 0.999" shows the effect of increasing the DP from the 0.99 used for the other curves. The resultant loss in sensitivity is only slightly more than 0.1 stellar magnitudes.

The top curve in Figure 6.7 illustrates the sensitivity obtained without signal integration (SAI or TDI). This curve was generated using the counts (signal and background) obtained in a single CCD frame. The detection probability per frame was taken to be 0.0684 which gives the probability of 0.99 for detecting the target in at least one of the 65 frames during which the target crosses the array. In order to maintain the total BER of 10^{-6} , the background event probability per frame had to be 65 times ($N_f = 65$) smaller than the corresponding BEP required when using signal integration. The loss in sensitivity when using single frame detection is approximately 1.7 stellar magnitudes under the conditions used here.

Assuming that the background is due only to zodiacal light,

the background count rate was converted to solar angle using the curves presented in Section 3.0. The resultant LTI vs solar angle curves are shown in Figure 6.8. The DP used for these results was 0.99 and observation times of 30 and 60 seconds were considered. Again, dashed lines are used to indicate regions for which the results may be inaccurate due to the small signals involved.

The extreme sensitivity of the ICCD is apparent from the results shown in Figure 6.8. Even relatively close to the sun, targets as weak as eighth magnitude can be detected. Farther from the sun, the sensitivity increases although the corresponding signals drop to a few photoelectrons per frame at about 35 degrees. Beyond 35 degrees, the sensitivity continues to increase and single photoelectron detection becomes important. For these signals, the effect of CCD readout noise may make the present analysis inaccurate, but should not change the basic conclusion that ninth magnitude targets are detectable in 30 sec and tenth magnitude in 60 sec.

ICCD 202
E = 0.75
DP = 0.99
I = 0.02 SEC.
Nx = 100

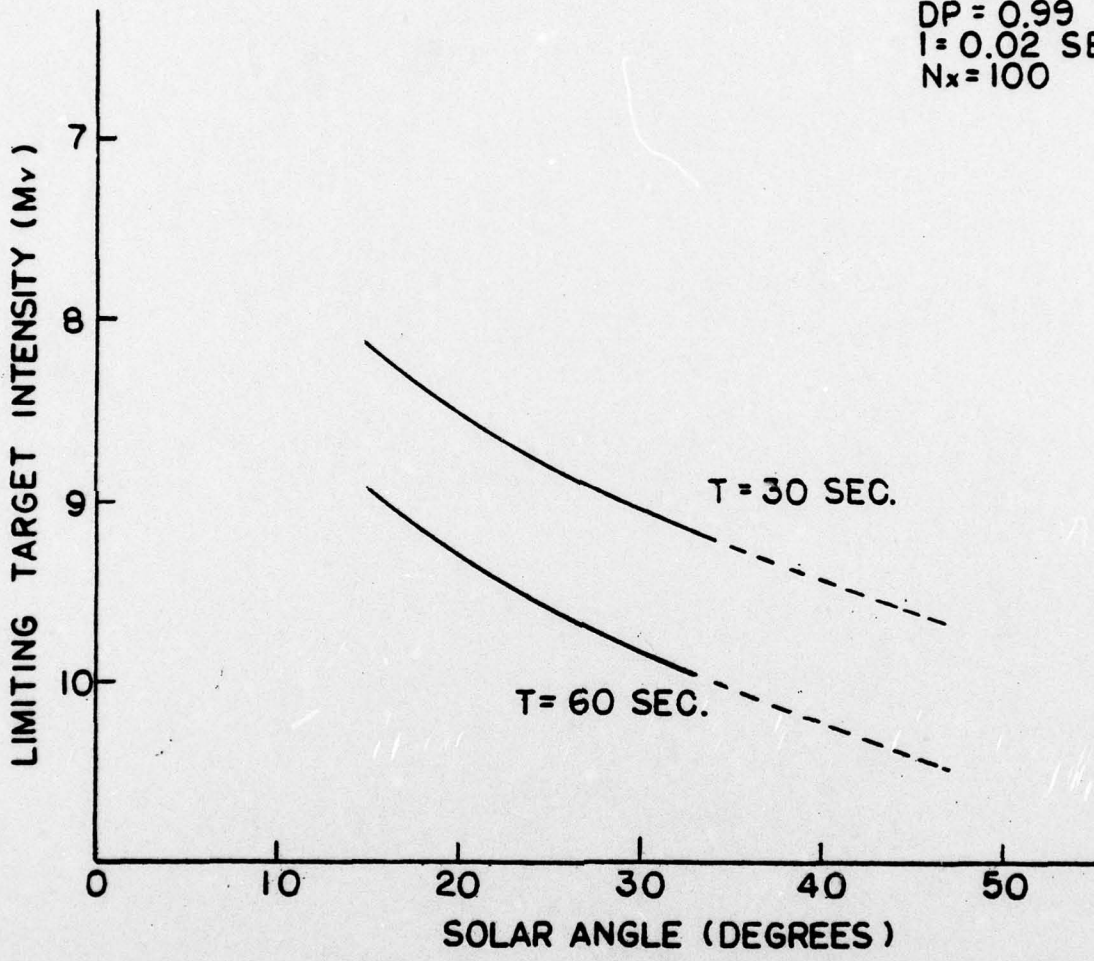


Figure 6.8. Limiting Target Intensity vs Solar Angle for Observation Times of 30 Sec. and 60 Sec.

REFERENCES

1. "Visible Terminal Warning Sensor," S. W. Kash and N. C. Chang, Aerospace Corporation Report No. TOR-0075 (5485)-1, January 8, 1975.
2. "Detecting Photoelectron Images with Semiconductor Arrays for Multichannel Photon Counting," J. P. Choisser, Optical Engineering, Vol. 16, No. 3, p. 262, May/June 1977.
3. "Astrophysical Quantities," Third Edition, C. W. Allen, Athlone Press, London, 1973.

ICCD SENSITIVITY INVESTIGATION

Glossary of Notation and Abbreviations

A	Effective aperture area of optics (m^2)
a	Width of photosensitive column (μm)
BEP	Background Event Probability; i.e., probability that the background count exceeds the detection threshold
BER	Background Event Rate: the rate at which background signals (no target) exceed the detection threshold
CCD	Charge Coupled Device
d	Width of transfer register column (μm)
DP	Detection Probability: the probability that the target signal will exceed the detection threshold
E	Geometrical efficiency factor to account for possible vertical misalignment between the target spot and the rows of pixels
F	Number of standard deviations between mean total count and threshold to produce a given detection probability
f _l	Telescope focal length (mm)
f#	Telescope f-number
I	CCD frame integration time (sec)
ICCD	Intensified Charge Coupled Device
k	Proportionality constant between N_e and S_e (ADC units/photoelectron)
LTI	Limiting Target Intensity: the target intensity which, (for a specified detection probability, produces a BER of 10^{-6} per second)
M	Mean number of counts for calculated Poisson Distribution
M_b	Background intensity (visual magnitudes per square degree)
m_v	Apparent visual magnitude of target
N_b	Total background accumulated as target spot crosses array (photoelectrons)

ICCD SENSITIVITY INVESTIGATION

Glossary of Notation and Abbreviations

N_e	Mean signal in distribution (photoelectrons)
N_f	Number of frames a target spot is on the array
N_p	Peak signal on one pixel (photoelectrons/pixel/frame)
N_s	Total signal accumulated as target spot crosses array (photoelectrons)
N_T	Total signal plus background accumulated (photoelectrons)
N_x	Number of columns of pixels in scan direction
N_y	Number of rows of pixels normal to scan direction
\bar{N}_b	Background intensity (photoelectrons/pixel/frame)
\bar{N}_s	Average signal as spot crosses CCD array (photoelectrons/pixel/frame)
n_b	Background count rate per pixel per scan
n_o	Signal intensity from a target (photoelectrons per second)
$n(t)$	Instantaneous signal on a pixel (photoelectrons/sec/pixel)
P	Scan speed (pixels/CCD frame time)
Q	Difference between the mean background count and the detection threshold (in units of $\sqrt{\bar{N}_b}$)
S	Scan speed (degrees/sec)
S_e	Mean signal in distribution (analog-to-digital converter (ADC) channel numbers)
SAI	Shift-and-Add Integration: a technique for off-chip integration of moving target signals
S_{int}	Total integrated signal on one pixel crossed by spot (photoelectrons)
T	Total time for one observation

ICCD SENSITIVITY INVESTIGATION

Glossary of Notation and Abbreviations

TDI	Time-Delay Integration: a technique for on-chip integration of moving target signals
THR	Threshold level for target detection (photoelectrons)
T'	Time for centroid of target spot to cross pixel (sec)
T#	Telescope T-number
v	Velocity of target spot across CCD array ($\mu\text{m}/\text{sec}$)
Δx	Pixel dimension in scan direction (μm)
Δy	Pixel dimension normal to scan direction (μm)
$\Delta\phi$	Pixel angular acceptance in scan direction (degrees)
$\Delta\theta$	Pixel angular acceptance normal to scan direction (degrees)
ϕ	Sensor field-of-view along scan direction (degrees)
ϕ_s	Angular extent of observed area along scan direction (degrees)
σ	Standard deviation of Gaussian approximation to signal distribution (photoelectrons)
σ_o	Signal standard deviation due to electronic noise (photoelectrons)
σ_s	Signal standard deviation due to photoelectron statistics (photoelectrons)
θ	Sensor field-of-view normal to scan direction (degrees)
θ_s	Angular extent of observed area normal to scan direction (degrees)

PRIMARY DISTRIBUTION LIST

Defense Documentation Center (DDC) Cameron Station Alexandria, VA 22314	12
Air University Library Maxwell AFB, AL 36112	1
HQ AFSC/DLCEA Andrews AFB, MD 20334 Attn: Dr. F. Jenkins	1
HQ AF/RDSD Washington, DC 20330 Attn: LtCol Bracken	1
AFAL/WRA-1 Library Wright-Patterson AFB, OH 45433 Attn: B. J. Sabo	1
AFAL/WRA Wright-Patterson AFB, OH 45433 Attn: LtCol Duggins	1
The Aerospace Corporation P O Box 92957 Worldway Postal Center Los Angeles, CA 90009 Attn: Dr. J. Reinheimer	1
Dr. S. Kash	2
N. C. Chang	1
R. B. Wood	1
R. F. Cannata	1
HQ SAMSO P O Box 92960 Worldway Postal Center Los Angeles, CA 90009 Attn: Col Randolph (YN)	1
Capt Turnipseed (YNV)	1